

Ultra-luminous Infrared galaxies in SDSS Data Release 6

L. G. Hou¹, Xue-Bing Wu², J. L. Han¹

ABSTRACT

Ultra-luminous infrared galaxies (ULIRGs) are interesting objects with dramatic properties. Much efforts have been made to understand the physics of their luminous infrared emission and evolutionary stages. However, a large ULIRG sample is still needed to study the properties of their central black holes (BHs), the black hole–host galaxy relation and their evolution. We identified 308 ULIRGs from the Sloan Digital Sky Survey Data Release 6, and classified them into the NL ULIRGs (with only narrow emission lines) and the Type I ULIRGs (with broad emission lines). About 56% of ULIRGs in our total sample show interaction features, and this percentage is 79% for redshift $z < 0.2$. Optical identifications of these ULIRGs show that the AGN percentage is at least 49%, and the percentage increases with the infrared luminosity. We found 62 Type I ULIRGs, and estimated their BH masses and velocity dispersions from their optical spectra. Together with known Type I ULIRGs in the literature, a sample of 90 Type I ULIRGs enables us to make a statistical study. We found that the BH masses of Type I ULIRGs are typically smaller than those of PG QSOs, and most Type I ULIRGs follow the $M_{\text{BH}} - \sigma$ relation. However, some ULIRGs with larger Eddington ratio deviate from this relation, even the line width of [OIII] narrow line core or [SII] line was used as the surrogate of velocity dispersion. This implies that at least some ULIRGs are probably still in the early evolution stage toward QSOs. The anti-correlation between the mass deviation from the $M_{\text{BH}} - \sigma$ relation and the Eddington ratio supports that the evolution of Type I ULIRGs is probably followed by the building up of the $M_{\text{BH}} - \sigma$ relation and the evolution to the QSO phase.

Subject headings: galaxies: infrared — galaxies: nuclei — galaxies: active — galaxies: starburst — galaxies: formation

¹National Astronomical Observatories, Chinese Academy of Sciences, Jia-20, DaTun Road, Chaoyang District, Beijing 100012, China

²Department of Astronomy, School of Physics, Peking University, Beijing 100871, China

1. Introduction

Ultra-luminous infrared galaxies (ULIRGs) were discovered by Infrared Astronomical Satellite (IRAS) in large numbers with infrared luminosity in $8 \sim 1000 \mu\text{m}$ greater than $10^{12} L_{\odot}$. The serious intrinsic obscuration for ULIRGs in optical, UV and even in Mid-IR and X-ray bands (Condon et al. 1991b) makes it difficult to clearly probe their physical properties by observations. There are probably more ULIRGs at high redshifts than in the local universe, and even more than optically bright QSOs (Lonsdale et al. 2006). In the last two decades, multi-wavelength studies on ULIRGs have significantly improved our understanding of these dramatic objects (see the review papers of Sanders & Mirabel 1996; Lonsdale et al. 2006).

Extremely high infrared luminosity of ULIRGs is dominated by starbursts, and sometimes with additional contribution from AGNs. Most ULIRGs are interacting systems undergoing a wide range of merger stages (e.g. Zou et al. 1991; Clements et al. 1996; Murphy et al. 1996; Surace et al. 2000; Farrah et al. 2001; Veilleux et al. 2002). ULIRGs with large luminosity or spectroscopic signatures of AGNs are most likely late-stage mergers (Veilleux et al. 2002). Observations of the molecular gas in ULIRGs (see Mirabel & Sanders 1988; Sanders et al. 1986, 1991; Gao & Solomon 2004) proved that high-density gases are reserved in compact nuclear region. The connection between ULIRGs and AGNs was also found from optical and mid-infrared spectra (e.g. Kim et al. 1998; Veilleux et al. 1997, 1999a,b). About 25% of ULIRGs present evidences of AGNs, and the percentage increases to $\sim 50\%$ when L_{IR} is greater than $10^{12.3} L_{\odot}$. Less than 10% ULIRGs have broad emission lines, which are so-called Type I ULIRGs (see Clements et al. 1996; Wu et al. 1998a,b; Zheng et al. 1999; Canalizo & Stockton 2001; Cui et al. 2001). ULIRGs and AGNs most probably have evolutionary connection. To understand such possible connection, Lonsdale et al. (2006) suggest that major mergers of gas rich galaxies first form a massive cool starburst dominated ULIRG, then a warm ULIRG phase is followed when a central AGN turns on inside the dust cocoon and heats the surrounding dust. The central AGN will evolve into an optically bright phase when it blows away the surrounding dust cocoon. The resulting stellar system will resemble a spheroid, so that the mass of central black hole of AGN (M_{BH}) is related to the stellar velocity dispersion σ . The $M_{\text{BH}} - \sigma$ relation might build up at that time. In this scenario, ULIRGs are in a pre-AGN phase. The typical BH mass of ULIRGs should be smaller, and the galaxy bulge may not have been constructed completely, compared with those of normal QSOs.

Kawakatu et al. (2006) used a sample of 8 Type I ULIRGs in the local universe with data of full width at half maximum (FWHM) of H_{β} and optical continuum luminosity $L_{\lambda}(5100\text{\AA})$ from Zheng et al. (2002) to estimate their BH masses and investigate the black hole–bulge

relation. They found that the Type I ULIRGs have systematically smaller BH masses in spite of having the comparable bulge luminosity as QSOs and elliptical galaxies. We notice that the FWHM of H_β given in Zheng et al. (2002) are the FWHM of the whole emission line profile, not the FWHM of broad line component which should be used in the estimation of BH mass. Therefore, Kawakatu et al. (2006) may underestimate the masses of BHs for these ULIRGs. Using a sample of sources mostly from Zheng et al. (2002), Hao et al. (2005) carried out a study on the Type I ULIRGs (named as IR QSOs in their paper), and concluded that the typical BH mass of Type I ULIRGs is smaller, and the typical Eddington ratio ($L_{\text{bol}}/L_{\text{Edd}}$) is larger than those of PG QSOs. At higher redshift, Borys et al. (2005) found that sub-millimeter galaxies have smaller BH masses than QSOs with respect to the same mass range of bulges. Alexander et al. (2008) concluded that sub-millimeter galaxies host BHs with a mass of $\log(M_{\text{BH}}/M_\odot) \approx 7.8$ in their sample. Because of the similarity of local ULIRGs and high redshift sub-millimeter galaxies on bright infrared luminosity, large amount of gas, and the interacting systems, the investigations on local ULIRGs could enlighten our understanding about the high redshift sub-millimeter galaxies.

A large ULIRG sample is needed to study their central BHs, the black hole–host galaxy relation and galaxy evolution. The best known samples of IRAS luminous and ultra-luminous infrared galaxies are the Bright Galaxy Sample of Soifer et al. (1987), updated into the Revised Bright Galaxy Sample by Sanders et al. (2003), the complete flux-limited IRAS 1 Jy sample (Kim & Sanders 1998), the 2 Jy sample of Strauss et al. (1990) and the FIRST/IRAS sample of Stanford et al. (2000). Since the Sloan Digital Sky Survey (SDSS) covers more than a quarter of the sky, more ULIRGs with relatively high quality spectra can be found by the cross-correlation of IRAS data with SDSS. Goto (2005) investigated the optical properties of 4248 infrared galaxies with L_{IR} of 10^9 to $10^{13.57} L_\odot$ from the cross-correlation between SDSS DR3 spectroscopic sample of galaxies and IRAS sources, and 181 of them are ULIRGs. Pasquali et al. (2005) used the SDSS DR2 data to study the optical properties of IRAS galaxies. Cao et al. (2006) identified 1207 luminous infrared galaxies and 57 ULIRGs from SDSS DR2 for a statistical study. Hwang et al. (2007) identified 324 ULIRGs from SDSS, 2dF Galaxy Redshift survey (Colless et al. 2001), and 6dF Galaxy Survey (Jones et al. 2004). Because the new SDSS spectroscopic sample of galaxies in DR6 has been released (Adelman-McCarthy et al. 2008), a larger ULIRG sample can be identified and then used to re-examine the statistical properties of ULIRGs.

This paper is organized as follows. In section 2, we make a cross-correlation between the IRAS Faint Source Catalogue and the spectroscopic catalogue of SDSS DR6, and obtain a ULIRG sample. We separate them into two sub-samples, NL ULIRGs and Type I ULIRGs, and fit their SDSS spectra. We present the results and discuss the NL ULIRG sample in section 3. In section 4, we carry out a study on the BH masses and the $M_{\text{BH}} - \sigma$ relation of

Type I ULIRGs. The discussions and conclusions are presented in section 5 and section 6. In this paper, we adopt $H_0 = 70 \text{ km s}^{-1} \text{ Mpc}^{-1}$, $\Omega_m = 0.3$ and $\Omega_\Lambda = 0.7$.

2. The ULIRG sample

SDSS DR6 spectra catalog contains about 750000 galaxies and QSOs and covers over 7425 deg^2 (Adelman-McCarthy et al. 2008). IRAS faint sources catalog (Moshir et al. 1992, hereafter FSC92) contains 173044 sources with IR flux in bands of 12, 25, 60 and $100 \mu\text{m}$. Although the IRAS dataset was published more than 17 years ago, it is still very under-explored. Only 43% of the total IRAS extragalactic FSC sources have been included in any sort of publication (Lonsdale et al. 2006).

The positional uncertainty of IRAS source (about $1 - 13 \text{ arcsec}$ for the in-scan direction and $3 - 55 \text{ arcsec}$ for the cross-scan direction) is much larger than that of object in SDSS DR6, and is described by an uncertainty ellipse. Similar to Hwang et al. (2007) and Cao et al. (2006), We used the positional uncertainty ellipse of each IRAS source to obtain their matched counterparts in the SDSS. If a galaxy of SDSS DR6 falls into the 3σ uncertainty ellipse of IRAS source, we regarded them as a match. As a result, we found that 11354 IRAS sources have only one counterpart in SDSS DR6 and 984 have more than one counterparts. In the later case, the likelihood ratio method (see Sutherland & Saunders 1992; Hwang et al. 2007; Cao et al. 2006) is used to determine which counterpart of this IRAS source is the most probable one. After doing these, we obtained a list of 12338 IRAS sources with SDSS DR6 optical counterparts.

2.1. Selection criteria

Our selection criteria of ULIRGs are shown as follows: For the 12338 matched IRAS sources, their $12 \mu\text{m}$ and $25 \mu\text{m}$ flux densities are mostly upper limits. Therefore, we calculated their far-infrared luminosity by using $60 \mu\text{m}$ and $100 \mu\text{m}$ fluxes with the following formulae (see Helou et al. 1988; Sanders & Mirabel 1996) and converted it to the total infrared luminosity (Calzetti et al. 2000):

$$F_{\text{FIR}} = 1.26 \times 10^{-14} \{2.58f_{60} + f_{100}\} [\text{Wm}^{-2}], \quad (1)$$

$$L_{\text{FIR}} = 4\pi D_L^2 F_{\text{FIR}} [L_\odot], \quad (2)$$

$$L_{\text{IR}}(1 - 1000\mu\text{m}) = 1.75 L_{\text{FIR}}. \quad (3)$$

Here f_{60} , f_{100} are the IRAS flux densities in Jy at 60 and 100 μm , D_L is the luminosity distance, F_{FIR} is the far infrared flux, L_{FIR} is the far infrared luminosity, and L_{IR} is the infrared luminosity in L_\odot . For all the matched sources, we also required that the 60 μm flux with flux quality = 3 (In the FSC92, high quality, moderate quality and upper limits of the flux measurements are marked as 3, 2, and 1 respectively). Because the 100 μm flux does not affect much on the value of L_{IR} (see Cao et al. 2006), we do not set the limit to the quality of 100 μm flux density. We also required that the redshift confidence of each source is larger than 0.65. We finally identified 325 ULIRG candidates with IR luminosity greater than $10^{12} L_\odot$. When we check these 325 ULIRG candidates by using the NASA/IPAC Extragalactic Database (NED), we found 18 sources whose redshifts provided in NED are not consistent with our results. According to the NED indentifications, 9 of these 18 sources have Petrosian r band magnitude less than 15, so they are too bright for SDSS. If calculated their L_{IR} with the redshifts provided in NED, we found that 17 of 18 sources are not ULIRGs. This discrepancy is probably due to the large position error of the IRAS sources and the incompleteness of the SDSS spectra. The fraction of the sources which are not excluded in the examination with NED (307/325) is about 94.5%, which is consistent with the reliability of our sample (about 93.4%, see the next section). By excluding these objects, we obtain a sample of 308 ULIRGs.

The distributions of redshift and infrared luminosity of ULIRGs are shown in Fig. 1. The redshifts of our ULIRG sample cover a range from about 0.03 to 0.6, with the median value of about 0.2, which is similar with that of Hwang et al. (2007).

We compared our result with that of Hwang et al. (2007), who identified 126 ULIRGs from SDSS DR4 but adopted different method to calculate L_{IR} . Our catalog recovers 122 of their 126 ULIRGs. For the rest 4 sources in their sample: F07568+4823 and F11553+4557 have IR luminosities of $10^{11.99} L_\odot$ in our result and thus are not selected; F10200+4839 and F15239+4331 are not ULIRGs, and wrong optical counterparts were identified by Hwang et al. (2007).

In order to obtain the radio properties of these ULIRGs, we also cross identified our ULIRG sample with the NVSS (Condon et al. 1998) and FISRT (Becker et al. 1995; White et al. 1997) catalogs. Note that Best et al. (2005) used a hybrid NVSS-FIRST method to identify the radio counterparts for SDSS DR2 galaxies with high reliability and completeness. We followed their method to identify radio counterparts of our ULIRG sample, and found that 140 of 308 ULIRGs have counterparts in the NVSS catalog within a typical searching radius about $15''$, and 132 of these 140 sources have FIRST counterparts within $3''$. Some of them are probably core-dominant radio sources, such as F08201+2801, F13408+4047, F16413+3954, F10418+1153, F09105+4108, F13451+1232, F11206+3639 and F08507+3636. For the rest

168 ULIRGs, 82 of them have one FIRST counterpart within $3''$, and their radio flux densities are below or close to the NVSS flux limit (about 2.5 mJy). The radio information of these 222 ULIRGs are listed in our ULIRG catalog (see Table 1).

2.2. Reliability estimated with the likelihood ratio method

To estimate the reliability of our sample, we follow Cao et al. (2006) and Hwang et al. (2007) and adopt a likelihood ratio method (Sutherland & Saunders 1992). The likelihood ratio p is defined as:

$$p = \frac{Q(\leq m_r) \exp(-R^2/2)}{2\pi\sigma_a\sigma_b n(\leq m_r)}. \quad (4)$$

$Q(\leq m_r)$ is the multiplicative factor measuring the probability for a true optical counterpart brighter than the flux limit exists in the association, and we set $Q = 1$ for simplicity. σ_a and σ_b are the standard deviations, and m_r is the SDSS r band magnitude. Here we assume the errors are Gaussian distributed (the error of an IRAS source is not a pure Gaussian, but in the statistical sense, the result of likelihood ratio study can still be used to evaluate the reliability), and define R as:

$$R^2 = \frac{(d_1)^2}{\sigma_{a1}^2 + \sigma_{a2}^2} + \frac{(d_2)^2}{\sigma_{b1}^2 + \sigma_{b2}^2}, \quad (5)$$

where d_1 and d_2 are the positional differences along the two axes of the error ellipse between each IRAS source and its SDSS counterpart, σ_{a1} and σ_{b1} are the errors of each IRAS source along x and y axes, σ_{a2} and σ_{b2} are the errors of each matched SDSS source along x and y axes. Because the positional error of a SDSS source is much smaller than that of an IRAS source, we only consider σ_{a1} and σ_{b1} .

In this work, we adopt the 3σ error ellipse as the match justification, thus $n(\leq m_r)$ can be obtained by use of the formula:

$$n(\leq m_r) = \frac{N(\leq m_r)}{9\pi\sigma_{a1}\sigma_{b1}}, \quad (6)$$

where $n(\leq m_r)$ is the total surface density of objects brighter than the candidate, and $N(\leq m_r)$ is the number of galaxies whose magnitude is less than or equal to m_r . Under the above considerations, we get:

$$p = \frac{9 \exp(-R^2/2)}{2N(\leq m_r)}, \quad (7)$$

here we use the r band Petrosian magnitude for galaxies of SDSS DR6 to calculate p of each source. To obtain the reliability, we adopt the method proposed by Lonsdale et al. (1998)

and Masci et al. (2001). The reliability of a source with p is given by

$$Re(p) = 1 - \frac{N_{random}(p)}{N_{true}(p)}. \quad (8)$$

The $N_{true}(p)$ represents the number of true associations, and $N_{random}(p)$ represents the number of random associations with a p , which can be derived by offsetting the positions of IRAS sources and re-calculating the associated sample. The numbers of true and random matched sources are 12338 and 813, then the reliability of our sample is about 93.4%. Thus we believe that our ULIRG sample is reliable enough to make a statistical study on the properties of NL ULIRGs and Type I ULIRGs. The distribution of the reliabilities for our 308 ULIRGs is shown in Fig. 2.

2.3. The optical images of ULIRGs

We examine the images of these 308 ULIRGs by use of the SDSS DR6 Image List Tool. Due to the limited resolution of SDSS image, we can only mark the ULIRGs with obvious interaction feature. ULIRGs are classified into (see Veilleux et al. 2002): class (I) with one nuclei but with tail features; class (II) have two identified nuclei and well-developed tidal tails or/and bridges; class (III) have two close or even overlapped nuclei, and their redshifts (almost in all cases, only one source in this system has spectral redshift measurements, and another/others have only SDSS photometric redshift data) are consistent. Examples are shown in Fig. 3. About 56% of ULIRGs in our total sample show obvious interaction features. Nearby ULIRGs show more clearly the interaction features, with the percentage of about 92% for $z < 0.1$, 84% for $z < 0.15$, and 79% for $z < 0.2$. The selection effect is obvious in the classification of interaction features of ULIRGs, because we can see the tails and two interacting galaxies at the maximum redshift about $z = 0.3$. Objects at various merger stages appear in our ULIRG sample. Some of them are still widely separated, and some are advanced mergers. The minimum separation between two nuclei in our sample is about $2''$. The imaging property is classified for each source in Table 1.

Detailed information of our ULIRGs is given in Table 1. Optical spectra of all 308 ULIRGs are available from the SDSS archive. This forms the largest sample of ULIRGs with optical spectra.

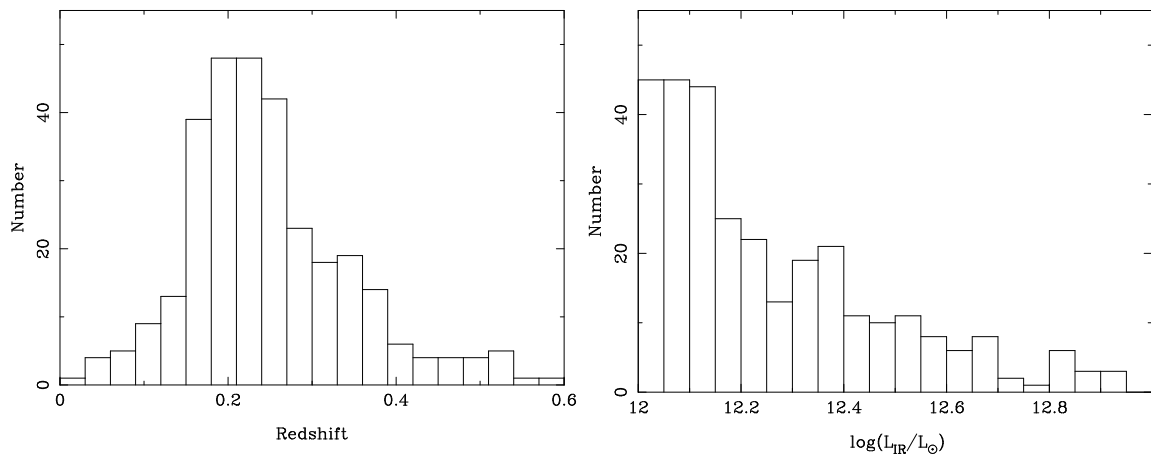


Fig. 1.— The distribution of redshift (left panel) and L_{IR} (right panel) of our ULIRG sample.

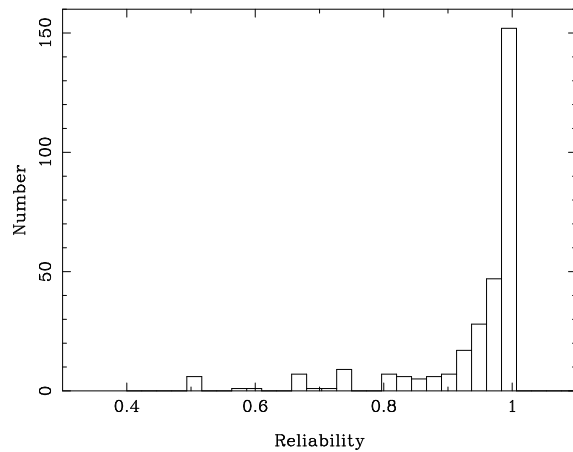


Fig. 2.— The distribution of source matching reliabilities of our ULIRG sample.

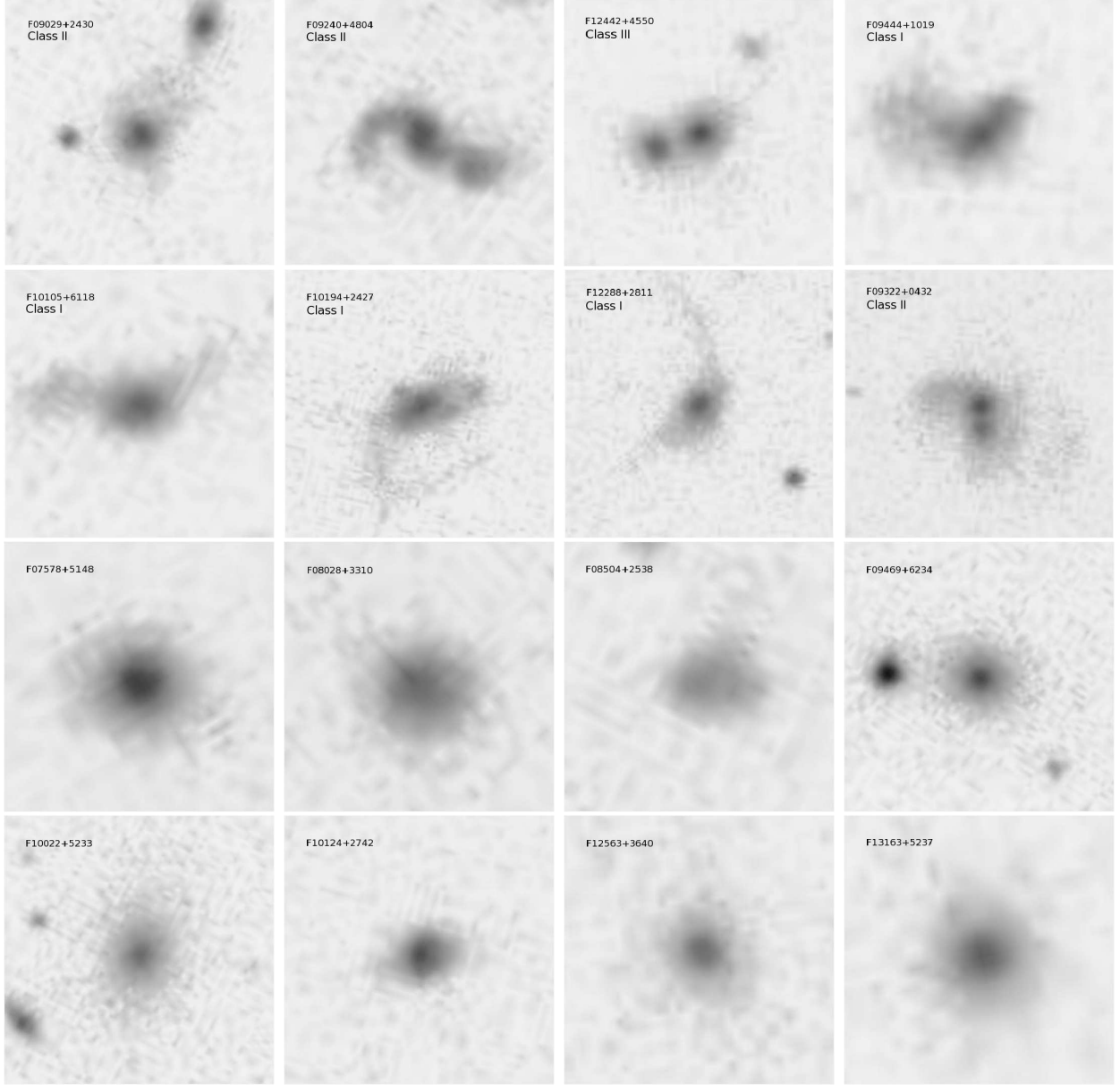


Fig. 3.— Examples of SDSS images of ULIRGs with (the upper eight) or without (the lower eight) obvious interacting features in our sample. The interaction classifications are labeled for the upper eight ULIRGs.

2.4. Optical spectra of ULIRGs

We want to identify Type I ULIRGs and NL ULIRGs from this sample. Only the spectra with $S/N > 3$ are considered in this study. After excluding the sources with no obvious emission lines in their spectra, we found 209 sources with emission lines, 62 of which have broad line component and are Type I ULIRGs.

SDSS spectra were processed as follows: First, we correct the Galactic extinction and redshift effects, then subtract the FeII emissions from the continuum by use of the optical iron template from Boroson & Green (1992) in the wavelength range $4250 \text{ \AA} < \lambda < 7000 \text{ \AA}$. Second, we fit the spectra using the Mpfitt package in IDL which is based on the Levenberg-Marquardt method. The continuum emission of ULIRGs comes from central AGN and host galaxy, and is often modified by the intrinsic dust extinctions. These effects should be considered for the determination of continuum flux. A local power-law is used to fit the continuum. After the subtraction of the fitted continuum emission from the spectra, we fit the emission lines. For NL ULIRGs, we use a single Gaussian profile to fit the H_α , H_β , [OIII]4959, 5007, [NII]6548, 6583, [SII]6716, 6731, and [OI]6300 emission lines. When a single Gaussian can not fit the profile of emission lines very well, double Gaussians are used to obtain the line flux. For Type I ULIRGs, we use two Gaussian components to fit H_α and H_β . If the [OIII] emission lines can not be well fitted by a single Gaussian, two Gaussian components are also used. Examples of the fitted spectra are given in Fig. 4.

3. NL ULIRGs

The emission line properties of 147 NL ULIRGs in our sample can be obtained and are listed in Table 1. We first classify them using the Baldwin-Phillips-Terlevich (BPT) diagram (Baldwin et al. 1981). (see Fig. 5).

The Balmer decrement method is often used to evaluate the intrinsic reddening effect. In previous works (e.g. Kewley et al. 2006; Veilleux et al. 1999a,b), $H_\alpha/H_\beta = 2.85$ was used for galaxies whose emission are dominated by star formation, and $H_\alpha/H_\beta = 3.1$ is used for galaxies dominated by AGN. But before we classify the object through the BPT diagrams, we can not assess which source is dominated by star formation or AGN. In this work, we adopt the intrinsic ratio $H_\alpha/H_\beta = 3.1$, and the reddening curve of Cardelli et al. (1989, hereafter CCM89), and also assume $R_v = A_v/E(B-V) = 3.1$ to do the optical classification. In order to examine the influence of intrinsic ratio of H_α/H_β , we also used $H_\alpha/H_\beta = 2.85$ to do the classification again, and found that classification of only one source (F09444+1019) is not consistent with the case of assuming $H_\alpha/H_\beta = 3.1$.

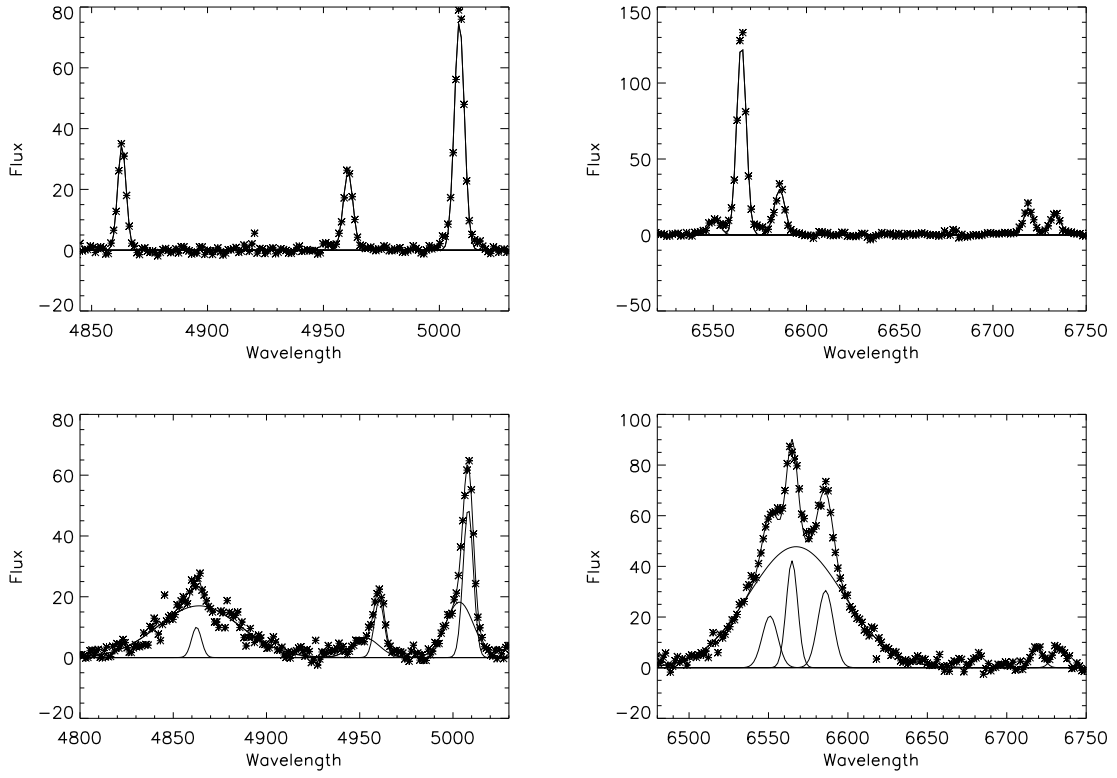


Fig. 4.— Examples of our fitted SDSS spectra for the H β and H α regions for a NL ULIRG (two upper panels) and a Type I ULIRG (two lower panels)

The intrinsic flux at wavelength λ can be expressed as:

$$I(\lambda) = F(\lambda) \times 10^{cf(\lambda)}, \quad (9)$$

The relation between the intrinsic and observed line ratio of H_α and H_β is:

$$I(H_\alpha)/I(H_\beta) = 10^{c(f(H_\alpha)-f(H_\beta))} \times F(H_\alpha)/F(H_\beta). \quad (10)$$

where $f(\lambda)$ is related to the generalized CCM89 reddening curve, $I(\lambda)$ is the intrinsic flux, $F(\lambda)$ is the observed flux, and c is the value of Balmer extinction. We estimated c from the observed line ratio and the reddening curve, after the intrinsic line ratio is assumed. We use the new classification scheme made by Kewley et al. (2006) for the classification. Each diagnostic line in the BPT diagram has been corrected using the above method.

The 147 NL ULIRGs are classified as five types: 29 Star-forming galaxies, 62 Composite galaxies (which are likely to contain metal-rich stellar populations, plus AGN, see Kewley et al. 2006), 34 Seyfert galaxies, 6 LINERs, and 16 ambiguous galaxies which are classified as one type in one or two diagrams but another type in the other diagram(s). Together with the 62 Type I ULIRGs, the percentage for AGNs is about 78% if we regard that the Composite galaxies also contain AGNs. The AGN percentage becomes 49% if we only consider the Seyfert galaxies, LINERs and Type I ULIRGs. The AGN percentage of ULIRGs increases with the infrared luminosity, consistent with the results in previous works (e.g. Veilleux et al. 1995, 1997; Wu et al. 1998b; Cao et al. 2006). The percentage (only consider the Seyfert galaxies, LINERs and Type I ULIRGs as AGNs) is 71% for ULIRGs with $L_{\text{IR}} > 12.3 L_\odot$, and 89% for $L_{\text{IR}} > 12.4 L_\odot$.

A tight correlation between far infrared and radio luminosities, covering about four orders of magnitude in the L_{IR} , has been found for infrared-selected galaxies (e.g. Helou et al. 1985; Yun et al. 2001). The non-thermal radiation from the relativistic electrons related with the supernova remnants is believed to be the main reason of this relation. Here, we verify this relation using our ULIRGs sample. FIRST flux density was used to calculate the radio luminosity. In our sample, 214 ULIRGs have FIRST counterparts, including 118 NL ULIRGs and 45 Type I ULIRGs.

The luminosities at $60 \mu\text{m}$ and at 1.4 GHz radio band are obtained using the following formulae (Yun et al. 2001):

$$\log L_{1.4\text{GHz}}(\text{WHz}^{-1}) = 20.08 + 2\log D + \log S_{1.4\text{GHz}}, \quad (11)$$

$$\log L_{60\mu\text{m}}(L_\odot) = 6.014 + 2\log D + \log S_{60\mu\text{m}}, \quad (12)$$

where D is the luminosity distance in Mpc, $S_{1.4\text{GHz}}$ and $S_{60\mu\text{m}}$ are flux densities in unit of Jy. The Radio–FIR relation of our ULIRGs is shown in Fig. 6. To examine the deviation of

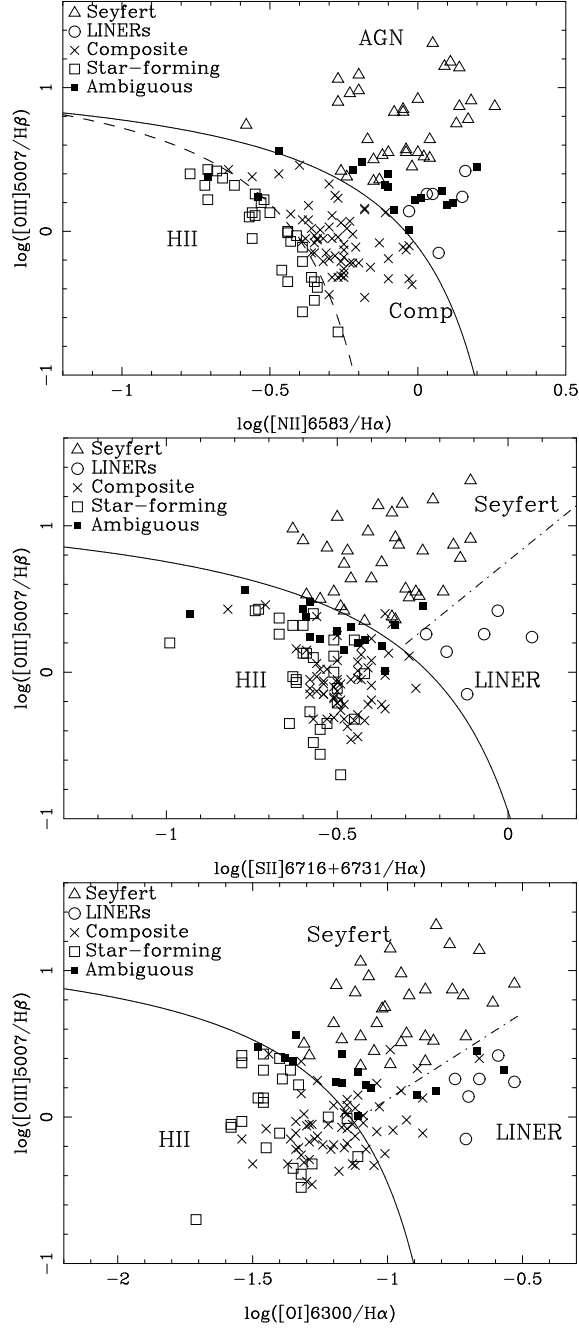


Fig. 5.— The BPT diagrams for 147 NL ULIRGs. The Balmer decrement method has been used to derive the extinction corrected flux of each emission line. Upper panel: The $[NII]/H\alpha$ versus $[OIII]/H\beta$ diagnostic diagram. The solid line is from Kewley et al. (2006), the dash line is from Kauffmann et al. (2003). Middle panel: The $[SII]/H\alpha$ versus $[OIII]/H\beta$ diagnostic diagram. The two lines are from Kewley et al. (2006). Lower panel: The $[OI]/H\alpha$ versus $[OIII]/H\beta$ diagnostic diagram. The two lines are from Kewley et al. (2006).

these ULIRGs from the linear relation, we also calculated the q parameter (see Condon et al. 1991a; Yun et al. 2001),

$$q = \log\left(\frac{2.58S_{60\mu\text{m}} + S_{100\mu\text{m}}}{2.98\text{Jy}}\right) - \log\left(\frac{S_{1.4\text{GHz}}}{\text{Jy}}\right). \quad (13)$$

A plot of q versus $L_{60\mu\text{m}}$ is shown in Fig. 7. The radio excess objects (i.e. the objects having 3 times larger radio flux density than the expected values from the linear Radio-FIR relation of Yun et al. (2001)) are AGNs, either Type I ULIRGs or Seyfert galaxies. Therefore the Radio-FIR relation originates from the starburst related non-thermal radiation, and the radio excess objects are due to AGN related radio emission (Roy & Norris 1997).

4. Type I ULIRGs

In our ULIRG sample, there are 62 Type I ULIRGs, We can explore their properties of central black holes. Examples of their SDSS spectra are shown in Fig. 8.

4.1. Black hole masses of Type I ULIRGs

We assume that the motion of the gas moving around the central black hole is dominated by the gravitation force and that the gas of Broad Emission Line Region (hereafter BLR) is virialized (e.g. Peterson & Wandel 1999, 2000). The BH mass can then be expressed as $M_{\text{BH}} = \frac{R_{\text{BLR}}V^2}{G}$, and the realistic formula given by Kaspi et al. (2000) is:

$$\frac{M_{\text{BH}}}{M_{\odot}} = 1.464 \times 10^5 \left(\frac{R_{\text{BLR}}}{\text{lt} - \text{days}}\right) \left(\frac{v_{\text{FWHM}}}{10^3 \text{kms}^{-1}}\right)^2, \quad (14)$$

where v_{FWHM} is the FWHM of broad emission line, and R_{BLR} is the radius of BLR. For our objects, the v_{FWHM} is taken as the FWHM of the broad component of H_{β} emission line, and the R_{BLR} can be estimated from the Fe II and Galactic extinction corrected continuum luminosity at 5100 Å, using:

$$\frac{R_{\text{BLR}}}{\text{lt} - \text{days}} = (26.4 \pm 4.4) \left[\frac{\lambda L_{\lambda}(5100\text{\AA})}{10^{44} \text{ergss}^{-1}}\right]^{(0.61 \pm 0.10)}. \quad (15)$$

The relation between R_{BLR} and $L_{\lambda}(5100\text{\AA})$ was first found by Kaspi et al. (2000), and their data was refitted by McLure & Jarvis (2002) in the same cosmology as we adopted. Here we assume that the central AGN dominates the continuum emission at 5100 Å, and the contribution from stellar emission and the intrinsic reddening effect can be neglected. Kawakatu et al.

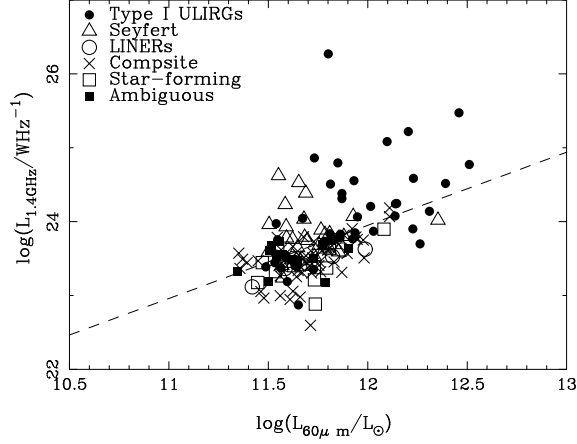


Fig. 6.— The 1.4 GHz radio luminosity vs. IRAS 60 μ m luminosity for our NL ULIRGs and Type I ULIRGs. The dashed line is the best fit given by Yun et al. (2001) from 1809 infrared galaxies.

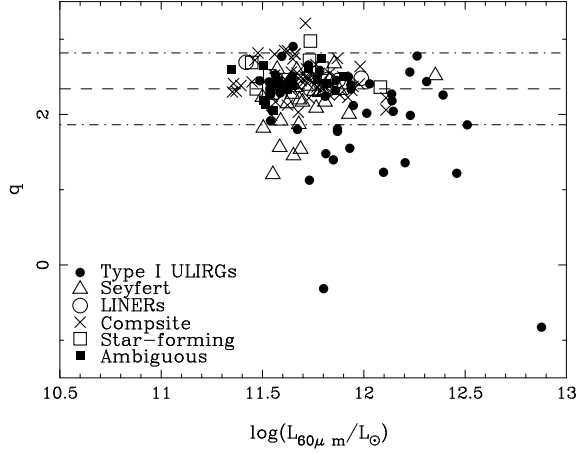


Fig. 7.— Distribution of q -values plotted with IRAS 60 μ m luminosity for the same sample used in Fig. 6. The dashed line marks the average value of $q = 2.34$ obtained by Yun et al. (2001), who used a sample of 1809 infrared galaxies. The two dot-dash lines represent 3 times larger radio (lower line) or IR (upper line) flux density than the expected values from the linear Radio-FIR relation of Yun et al. (2001).

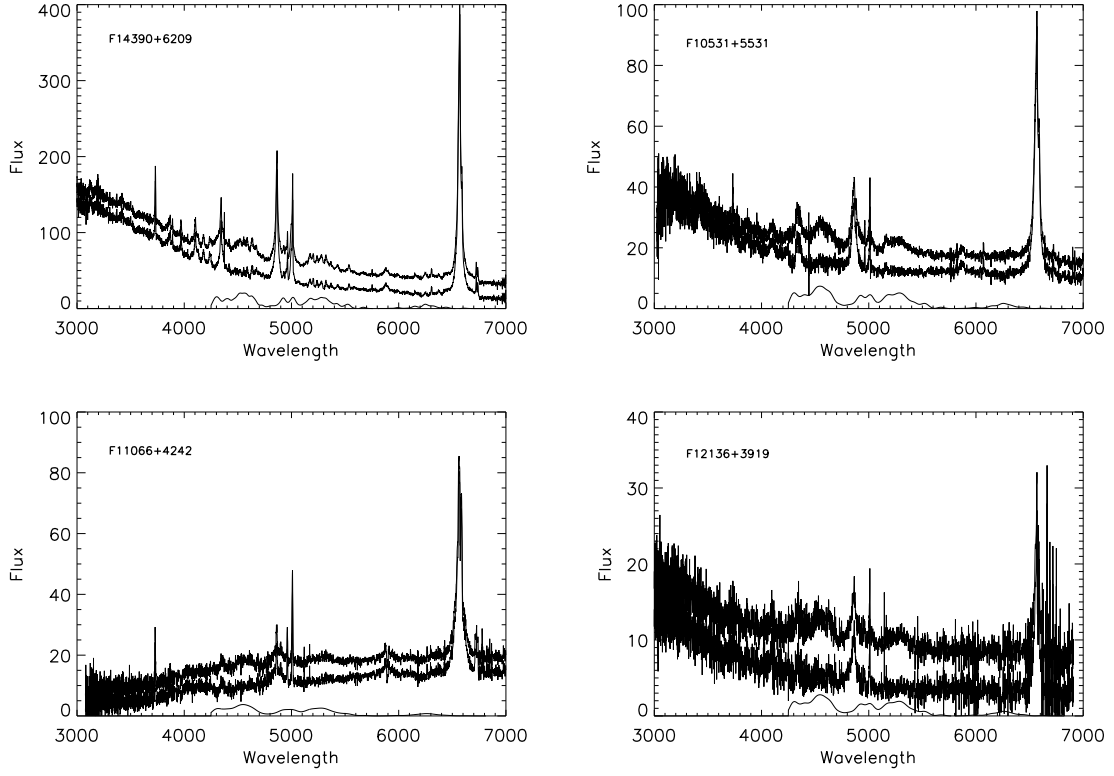


Fig. 8.— Examples of SDSS spectra of Type I ULIRGs in our sample. In each panel, the top curve is the extinction and red-shift corrected spectra. The middle curve is the spectra after the subtraction of the Fe II emissions, which was shifted downward. The bottom curve is the model for Fe II emissions.

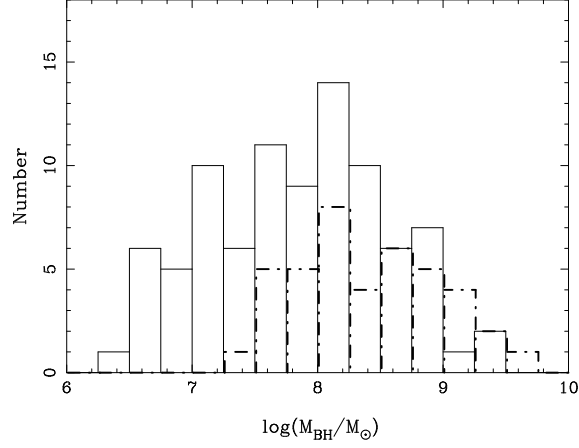


Fig. 9.— BH mass distribution. The solid line represents the BH mass distribution of our sample and the Type I ULIRGs from Hao et al.(2005), while the dot-dash line is for that of the PG QSOs obtained from Hao et al.(2005).

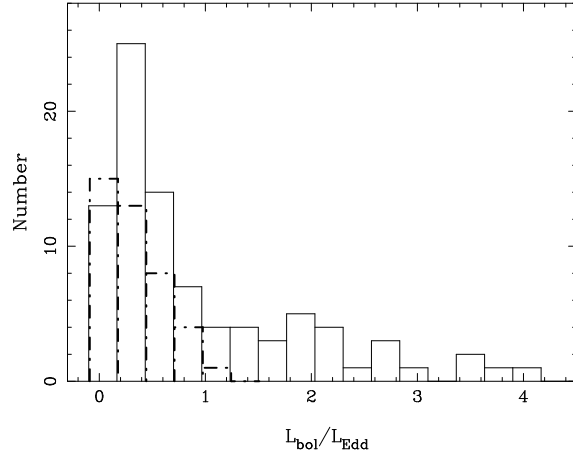


Fig. 10.— The Eddington ratio distribution of 90 Type I ULIRGs from our sample and Hao et al. (2005), while the dot-dash line is for that of the PG QSOs obtained from Hao et al.(2005)

(2006) argued that, for Type I ULIRGs, the central AGN dominance of the 5100 Å emission is reasonable.

To investigate the BH masses of Type I ULIRGs systematically, a large sample is absolutely needed. Kawakatu et al. (2006) used 8 ULIRGs from the Type I ULIRG sample of Zheng et al. (2002) to investigate this problem, and concluded that the BH masses of Type I ULIRGs are typically smaller than those of PG QSOs. The $\text{FWHM}_{\text{H}\beta}$ they used is not the broad component of $\text{H}\beta$, which leads to an underestimation of the BH mass. Hao et al. (2005) carried out a study on Type I ULIRGs, with a sample mainly from Zheng et al. (2002), but added several PG QSOs. The FWHM of $\text{H}\beta$ broad component they used was estimated in the same way as that in Boroson & Green (1992), who used double components to fit the $\text{H}\beta$ line. Hao et al. (2005) used the cosmology of $H_0 = 70 \text{ km s}^{-1} \text{ Mpc}^{-1}$, $\Omega_m = 0.3$ and $\Omega_\Lambda = 0.7$, same as ours. We noticed that 3 of our 62 Type I ULIRGs were listed in their sample: For F01572+0009, the BH mass in our work ($\log(M_{\text{BH}}/M_\odot) \sim 8.0$) is consistent with their result ($\log(M_{\text{BH}}/M_\odot) \sim 7.7$). For F10026+4347, the same BH mass ($\log(M_{\text{BH}}/M_\odot) \sim 7.8$) is given in Hao et al. (2005) and our work. But for the other source F13342+3932, the BH mass we got ($\log(M_{\text{BH}}/M_\odot) \sim 8.4$) is larger than theirs ($\log(M_{\text{BH}}/M_\odot) \sim 7.4$), mainly because we use the much broad component of $\text{H}\beta$ from SDSS spectra.

We combine the sample of Hao et al. (2005) with ours, and obtain a large sample of 90 Type I ULIRGs. The distribution of BH mass of this sample is shown in Fig. 9, compared with that of PG QSOs. Obviously, the BH masses of Type I ULIRGs (with a mean value of $6.7 \times 10^7 M_\odot$ for these 90 Type I ULIRGs and about $7.6 \times 10^7 M_\odot$ for our 62 Type I ULIRGs) are systematically smaller than those of PG QSOs (with a mean value of $2 \times 10^8 M_\odot$), consistent with the popular evolutionary scheme that ULIRGs are in a pre-QSO phase and their central BHs are still under growing.

The bolometric luminosity L_{bol} measures the total luminosity associated with AGN. We estimate the bolometric luminosity using the formula in Kaspi et al. (2000): $L_{\text{bol}} \approx 9\lambda L_\lambda(5100\text{\AA})$. For those ULIRGs from Hao et al. (2005), we directly use their data because they used the same methods to calculate the BH mass and L_{bol} . The distribution of Eddington ratio of this sample is shown in Fig. 10, and the mean value is about 0.92 for these 90 Type I ULIRGs, and 0.55 for our 62 Type I ULIRGs, larger than that of PG QSOs (the mean value of Eddington ratio for them is about 0.2).

The intrinsic reddening effect in Type I ULIRGs is still poorly known, and it probably affects the estimation of optical luminosity. The Balmer decrement method is often used to estimate the reddening effect for narrow emission galaxies, but is seldom used for broad emission line galaxies. In principle, the observations in X-ray band can be used to estimate the absorption column density and then the absorption. But for our 62 Type I ULIRGs,

only several have been observed in X-ray band. More work is still needed to understand the intrinsic reddening effect in Type I ULIRGs.

4.2. The $M_{\text{BH}} - \sigma$ relation for Type I ULIRGs

The $M_{\text{BH}} - \sigma$ relation for ULIRGs was seldom discussed in the past, mainly due to the poor understanding of BH masses and the limitation of sample size. Dasyra et al. (2006b) measured the velocity dispersions of 54 ULIRGs, and carried out a simulation to study the reasonableness of using the $M_{\text{BH}} - \sigma$ relation to estimate their BH masses. They concluded that if the efficiency of gas accretion onto the BH from its surroundings remains constant with time, this relation can be used. For Type I ULIRGs, we can estimate their BH masses and velocity dispersions by use of their optical spectra, thus it's possible to test the $M_{\text{BH}} - \sigma$ relation for ULIRGs *by observation*. Here we investigate the $M_{\text{BH}} - \sigma$ relation for our Type I ULIRG sample.

When the stellar velocity dispersions have measured data in the literature, we adopt them directly, otherwise, the line width of some narrow emission lines, such as [OIII]5007, [OIII]5007 narrow line core, [SII]6716 or 6731, are used to be the surrogates for σ , which were usually adopted in the studies on different type of AGNs (e.g. Nelson 2000; Boroson 2003; Grupe & Mathur 2004; Salvander et al. 2007; Komossa & Xu 2007). For six sources, F01572+0009, F12540+5708, F15462–0450, F21219–1757, F13451+1232(w) and PG 0050+124, their velocity dispersions have been measured in Dasyra et al. (2006a,b, 2007), and are directly adopted here. In the estimation of BH mass uncertainty, we considered the uncertainty of the formula (Eq. 15), the errors of the $L_{\lambda}(5100\text{\AA})$ and $\text{FWHM}_{\text{H}\beta}$. The uncertainty of σ is estimated from the fitting error of FWHM of emission lines, and the instrumental resolution of σ for SDSS spectra is about 70 km s^{-1} . To make a comparison, we also use the value of 7 QSOs from Dasyra et al. (2007), who measured the σ for 11 QSOs. Among these 11 QSOs, PG0050+124 is identified as a Type I ULIRG and PG1404+226 as a narrow line Seyfert 1 galaxy in Hao et al. (2005). PG1426+015 is an interacting system. The BH mass of LBQS0307–0101 is unavailable. Thus only 7 of 11 QSOs are used, and the instrumental resolution for their measured velocity dispersion is about 30 km s^{-1} .

We show the $M_{\text{BH}} - \sigma$ relation of our sample by use of these surrogates of σ in Fig. 11, where $\sigma = \text{FWHM}_{\text{lines}}/2.35$. Because the outflow may influence the profile of [OIII], there are some problems when using the FWHM of [OIII]5007 profile as the surrogate of σ . Thus we do not adopted the FWHM of [OIII]5007 profile as the surrogate of σ . In the upper panel, the FWHM of [OIII] narrow line core is used to estimate σ . Komossa & Xu (2007) used [SII] as the surrogate of σ and found that narrow-line Seyfert 1s do follow the $M_{\text{BH}} - \sigma$

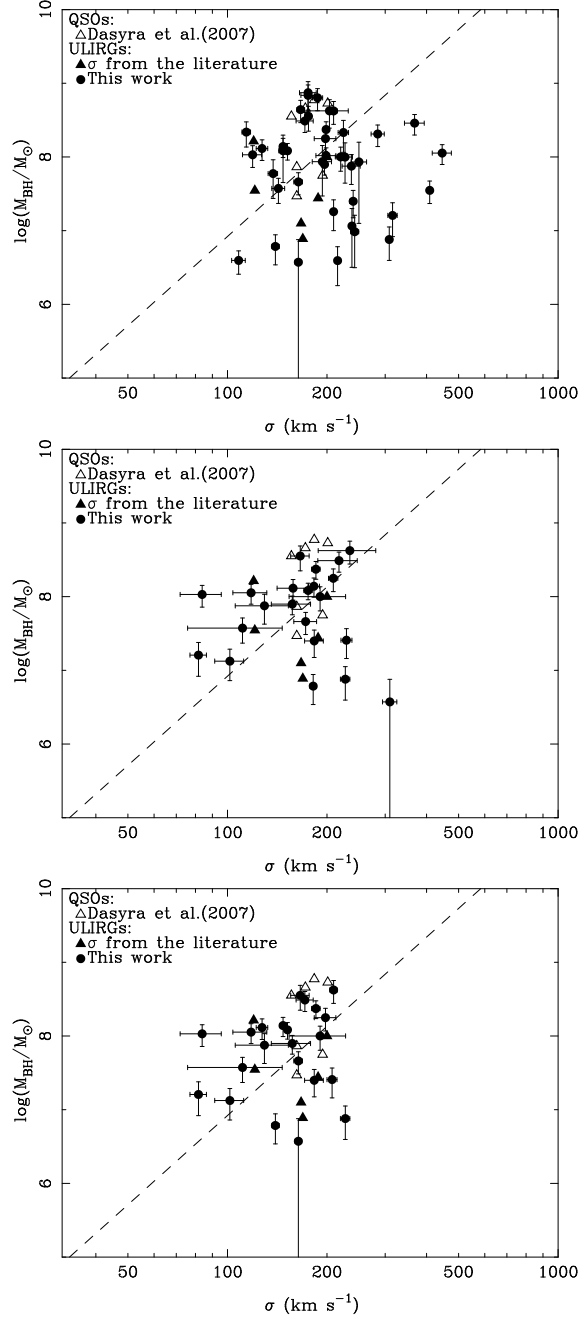


Fig. 11.— The $M_{\text{BH}} - \sigma$ diagrams for Type I ULIRGs. The filled triangles represent the six sources with measured σ in Dasyra et al. (2006a,b, 2007), open triangles represent the 7 QSOs with measured σ in Dasyra et al. (2007), filled circles indicate the ULIRGs whose parameters are estimated in this work. If σ is unavailable in reference, it was estimated by several methods: Upper panel, the σ is estimated from FWHM of [OIII] narrow line core; Middle panel, the σ is estimated from FWHM of [SII] profile; Lower panel, the same as middle panel, except that for some sources, i.e. F11394+0108 and F17234+6228, their velocity dispersions are estimated from the FWHM of [OIII] narrow line core because the FWHM of [OIII] NL core is smaller than that of [SII] profile. The dashed line is the $M_{\text{BH}} - \sigma$ relation from Tremaine et al. (2002).

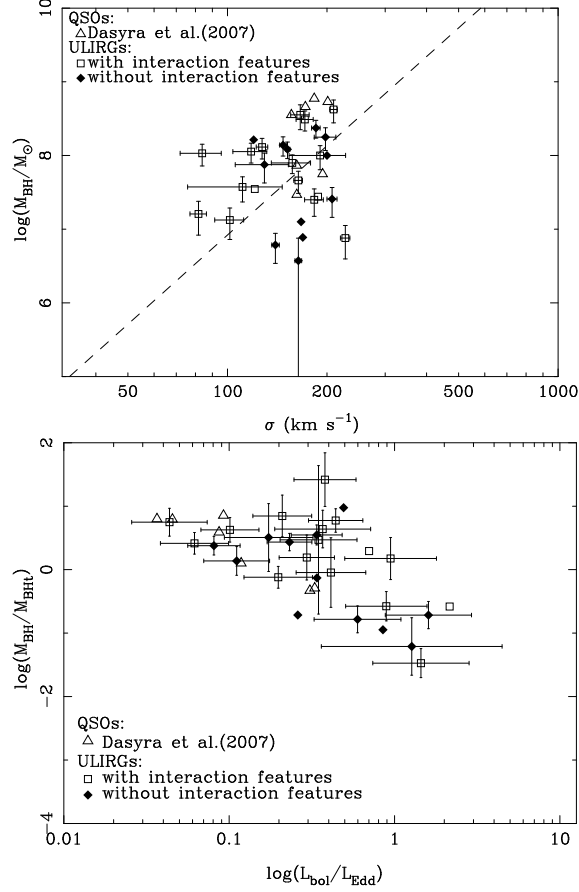


Fig. 12.— The $M_{\text{BH}} - \sigma$ and $\log(M_{\text{BH}}/M_{\text{BHt}})$ versus $\log(L_{\text{bol}}/L_{\text{Edd}})$ diagrams for ULIRGs with or without obvious interaction features. The open squares represent the sources with interaction features, filled rhombuses represent the ULIRGs without interaction features, and open triangles indicate the QSOs with measured σ in Dasyra et al. (2007).

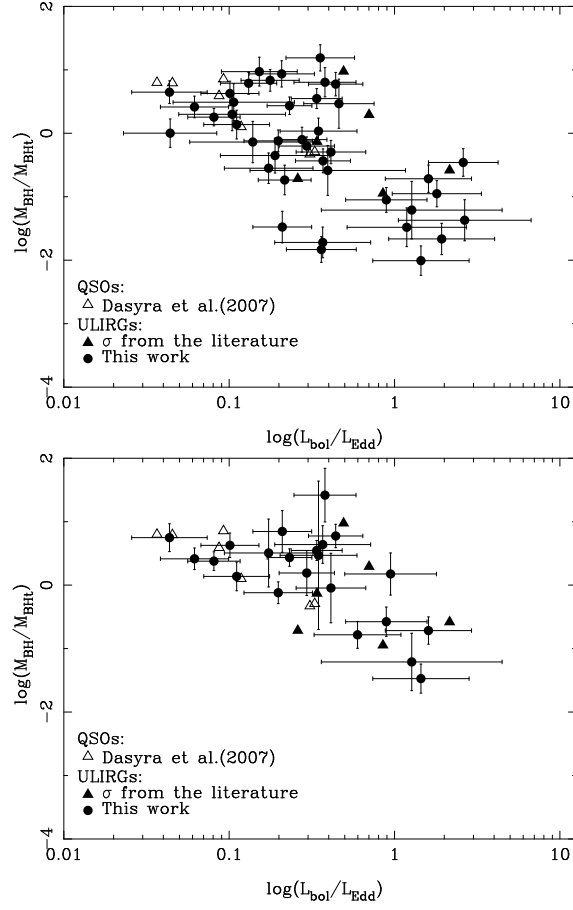


Fig. 13.— The $\log(M_{\text{BH}}/M_{\text{BHt}})$ versus $\log(L_{\text{bol}}/L_{\text{Edd}})$ relation of Type I ULIRGs. The filled triangles represent the six sources with measured σ in Dasyra et al. (2006a,b, 2007), open triangles represent the 7 QSOs with measured σ in Dasyra et al. (2007), the filled circles indicate the ULIRGs whose parameters are estimated in this work. Upper panel, the M_{BHt} is derived from the σ used in the upper panel of Fig. 11; Lower panel, The M_{BHt} is obtained from the σ used in the lower panel of Fig. 11.

relation. In the middle panel, we use the FWHM of [SII] to derive σ for some ULIRGs with well measured FWHM of [SII]. Some ULIRGs do not follow the $M_{\text{BH}} - \sigma$ relation well. We check the sources with larger deviations from this relation, and found that for some sources, i.e. F11394+0108 and F17234+6228, their FWHM of [SII] are broader than those of [OIII] profile, thus the FWHM of [OIII] narrow line core is used to estimate σ for these ULIRGs and the result is shown in the lower panel of Fig. 11. When considering the error bars, it seems that most ULIRGs follow the $M_{\text{BH}} - \sigma$ relation, but several sources still have relatively larger deviations compared with those 7 QSOs, which can be seen even from those six ULIRGs with measured velocity dispersions. Base on above discussions, we think that most Type I ULIRGs follow the $M_{\text{BH}} - \sigma$ relation, they are probably in a late evolutionary stage, but several ULIRGs do not follow this relation well, which probably hints that AGN phase appears in the late evolutionary stage of ULIRGs, and the $M_{\text{BH}} - \sigma$ relation of most Type I ULIRGs have already build up. According to the popular evolutionary picture of ULIRGs, in the evolution phase of ULIRGs to QSO, their BHs are growing, and the $M_{\text{BH}} - \sigma$ relation may be built up step by step. The scatter in the $M_{\text{BH}} - \sigma$ diagram is probably due to the fact that ULIRGs locate in different evolutionary stages and the central BHs of some ULIRGs are still rapidly growing. Therefore, the interaction properties of these Type I ULIRGs is helpful to understand this problem.

In our sample, F13451+3932 is an interaction system with two bright nuclei, BH mass and velocity dispersion can be obtained for the west component. F10531+5531 and F15529+4545 are interaction systems. F14394+5332 is interacting with a companion galaxy. Some sources show tidal tail/plume features or interacting with a much smaller galaxy, such as F01572+0009, F09591+2045, F11162+6020, F07548+4227, F11134+0225, F14026+4341, F14315+2955, F14390+6209 F11206+3639, F11394+0108, F13342+3932, F15320+0325, F15437+4647, F16122+1531, F17234+6228. Some Type I ULIRGs are probably interacting systems but not certain because of the lower image resolution and the lack of redshift data of their companions, such as F11553–0259, F10015–0018, F14402+0108. Other ULIRGs do not show obvious interaction features at least from their SDSS images. We compare those ULIRGs with or without interaction features in the $M_{\text{BH}} - \sigma$ diagram. The result is shown in Fig. 12. It seems that the ULIRGs with interaction features have slightly larger deviations, but the difference is not significant. Even for those ULIRGs with interaction features, some of them are close to the $M_{\text{BH}} - \sigma$ line, and others have larger deviations, which implies that the $M_{\text{BH}} - \sigma$ relation for some Type I ULIRGs is not fully built up. The sources in our sample do not show large deviations from the $M_{\text{BH}} - \sigma$ line, probably because the AGN phase appears in the late stage of mergers, and the interaction between central BH and its host galaxy already starts before the ULIRGs present broad emission lines in the optical band. More observations are needed to verify the interaction properties and merger stages

of all these Type I ULIRGs.

4.3. Dependence on Eddington ratio

We show the $\log(M_{\text{BH}}/M_{\text{BHt}})$ versus $\log(L_{\text{bol}}/L_{\text{Edd}})$ diagram in Fig. 13, where M_{BHt} is the BH mass calculated from the $M_{\text{BH}} - \sigma$ relation of Tremaine et al. (2002). Thus $\log(M_{\text{BH}}/M_{\text{BHt}})$ represents the deviation of BH mass from the $M_{\text{BH}} - \sigma$ relation. The Eddington ratio $\log(L_{\text{bol}}/L_{\text{Edd}})$ usually measures the accretion rate of BH. The uncertainty of $\log(M_{\text{BH}}/M_{\text{BHt}})$ is estimated from the uncertainties of M_{BH} , the $M_{\text{BH}} - \sigma$ relation of Tremaine et al. (2002) and σ . The uncertainty of $\log(L_{\text{bol}}/L_{\text{Edd}})$ is estimated from the errors of M_{BH} and $f_{5100\text{\AA}}$. An anti-correlation trend appears in this plot even we use different methods to estimate σ . For the sources with larger deviations from the $M_{\text{BH}} - \sigma$ relation, they tend to have larger Eddington ratios and smaller BH masses, implying that their BHs grow faster. For the sources which are close to the $M_{\text{BH}} - \sigma$ relation, they have relatively smaller Eddington ratios and larger BH masses, their central BHs grow slowly. These results imply that different kinds of ULIRGs probably exist (i.e. some are close to the $M_{\text{BH}} - \sigma$ relation and with relatively smaller Eddington ratio, some with larger deviations to the $M_{\text{BH}} - \sigma$ relation and relatively larger Eddington ratio), and they may have evolutionary connection. One possible explanation of this trend is that the merger of gas-rich galaxies will first form a non-regular host galaxy with a larger deviation from the $M_{\text{BH}} - \sigma$ relation. As the evolution of the central BH, the interaction between central BH and its host galaxy will result in a $M_{\text{BH}} - \sigma$ relation. As the Eddington ratio becomes smaller, the central BH becomes bigger and the stars around the central region form a regular spheroid step by step. In Fig. 12, we also plot the $\log(M_{\text{BH}}/M_{\text{BHt}})$ versus $\log(L_{\text{bol}}/L_{\text{Edd}})$ relation for ULIRGs with or without obvious interaction features, and it seems that no obvious difference appears.

In the estimation of M_{BH} and $L_{\text{bol}}/L_{\text{Edd}}$, we both used the continuum flux at 5100\AA . One may think that the trend appeared in the $\log(M_{\text{BH}}/M_{\text{BHt}})$ versus $\log(L_{\text{bol}}/L_{\text{Edd}})$ plot is due to the common dependence of these two quantities on the continuum flux at 5100\AA . Because $\log(M_{\text{BH}}/M_{\text{BHt}})$ is proportional to $\log(L_{5100\text{\AA}}^{0.61})$ (we used the R-L relation of Kaspi et al. 2000), and $\log(L_{\text{bol}}/L_{\text{Edd}})$ is proportional to $\log(L_{5100\text{\AA}}^{0.39})$. If the relation depends on the methods of estimating M_{BH} and $L_{\text{bol}}/L_{\text{Edd}}$, $\log(M_{\text{BH}}/M_{\text{BHt}})$ should increase as the increase of $\log(L_{\text{bol}}/L_{\text{Edd}})$. However, this is not the case in our plot. Therefore, we believe that the anti-correlation trend between $\log(M_{\text{BH}}/M_{\text{BHt}})$ and $\log(L_{\text{bol}}/L_{\text{Edd}})$ is robust.

Another important issue is the reliability of our Type I ULIRG sample. For 41 of these 62 Type I ULIRGs, their counterparts and redshifts listed in NED are consistent with our results. As for other 21 ULIRGs, no counterparts and redshifts are available in NED. We

check their reliability (discussed in section 2.3 and also see Fig. 2), and found that for 18 of these 21 ULIRGs, their reliability are greater than 93%. Because the large position error of IRAS measurement, and the incompleteness of SDSS spectra, several ULIRGs identified in this work may be problematic. However, this effect will not affect the statistical results about the NL ULIRGs. But for Type I ULIRGs, as we only have a small sample, this effect is probably important. To confirm this, we use 41 ULIRGs which are listed in NED and 6 ULIRGs from the literature (Dasyra et al. 2006a,b, 2007) to re-do the same work about Type I ULIRGs. We found that our results do not change, and some examples are shown in Fig. 14.

4.4. L_{IR} versus $\lambda L_{\lambda}(5100\text{\AA})$ relation

The relation between IR and optical continuum luminosities is helpful to understand the origin of the IR emissions in galaxies. Here we directly take the samples of Hao et al. (2005) to make a comparison, because they used the same cosmology as ours, although their calculation of L_{IR} is not consistent with ours (but the difference is very small, about 2%). We show the L_{IR} versus $\lambda L_{\lambda}(5100\text{\AA})$ diagram in Fig. 15. There is a tight correlation between the L_{IR} and $\lambda L_{\lambda}(5100\text{\AA})$ for PG QSOs and narrow line Seyfert 1 galaxies. The distribution of our 62 Type I ULIRGs is consistent with that of Hao et al. (2005), and most Type I ULIRGs are above the trend defined by the PG QSOs and narrow line Seyfert 1 galaxies. If this correlation can be explained as both the L_{IR} and $\lambda L_{\lambda}(5100\text{\AA})$ of PG QSOs and narrow line Seyfert 1 are mainly associated with AGN, the deviation to this correlation may imply that an additional contribution to the L_{IR} besides AGN in Type I ULIRGs, i.e. the contribution from starbursts.

5. Discussions

The intrinsic extinction of ULIRGs is significant. Kawakatu et al. (2006) estimated the optical extinction of three Type I ULIRGs using the X-ray data, and concluded that the optical extinction A_V is probably less than 1. While the typical optical extinction estimated from the Balmer decrement method for the NL ULIRGs is about 3 (see the $E(B-V)$ values provided in Veilleux et al. 1999a, and under the assumption of $R = A_V/E(B-V) = 3.1$). This result proves that the optical extinction of Type I ULIRGs is typically smaller than that of NL ULIRGs. We compared the optical extinction obtained from X-ray method and Balmer decrement method for these three Type I ULIRGs. For F11598–0112, the optical extinctions derived by these two methods are consistent with each other, both being about

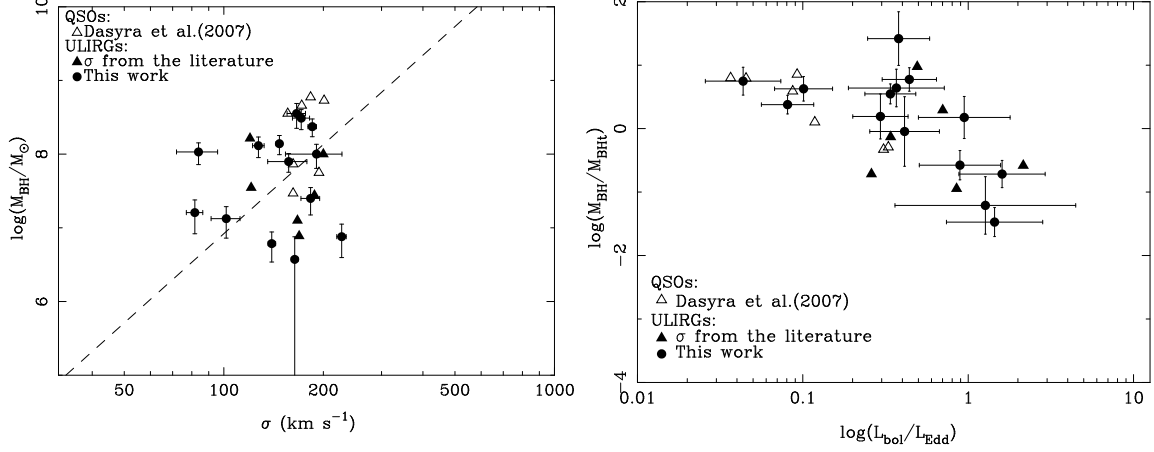


Fig. 14.— Two examples about the same results in Fig. 11 and Fig. 13, but only the data have been confirmed in previous works were used. Left panel: the same figure as the lower panel in Fig. 11. Right panel: the same figure as the lower panel in Fig. 13. The symbols of the left panel and the right panel represent the same objects as those in Fig. 11 and Fig. 13 respectively.

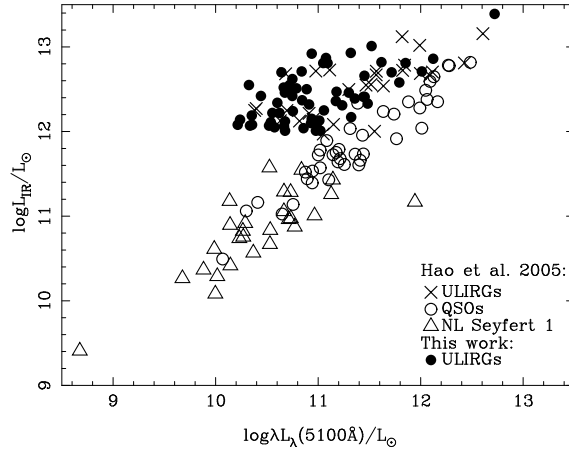


Fig. 15.— L_{IR} versus $\lambda_{\text{L}}(5100\text{\AA})$. Open circles indicate the PG QSOs, open triangles represent the narrow line Seyfert 1 galaxies, and crosses denote the Type I ULIRGs. All of the above data are from Hao et al. (2005). Filled circles represent new data of the Type I ULIRGs in our sample.

0.03. For F01572+0009, these two methods both give smaller values of optical extinction. For the remaining one F11119+3257, the extinctions derived by two methods have large difference. The extinction effect in different evolutionary stages may have large difference.

Recently, Dong et al. (2008) carried out a study on the broad line Balmer decrement in Seyfert 1 galaxies and QSOs, and concluded that the Balmer decrement is a good indicator for dust extinction. We use the Balmer decrement method to test the influence of extinction on our results. After such a correction, the mean BH mass of our Type I ULIRGs sample becomes $\log(M_{\text{BH}}/M_{\odot}) \approx 8.1$, which is larger than $\log(M_{\text{BH}}/M_{\odot}) \approx 7.8$ obtained without this correction, and is still typically smaller than that of PG QSOs ($\log(M_{\text{BH}}/M_{\odot}) \approx 8.4$). The anti-correlation trend appeared in the $\log(M_{\text{BH}}/M_{\text{BHt}})$ versus $\log(L_{\text{bol}}/L_{\text{Edd}})$ plot still exists. Therefore, we believe that the optical extinction does not affect our main results significantly.

In Fig. 11 and Fig. 13, we notice that the sources which are close to the $M_{\text{BH}} - \sigma$ relation tend to have relatively smaller Eddington ratios and larger BH masses. The distributions of their BH masses and Eddington ratios are similar with those of PG QSOs (see the upper panel in Fig. 13). For the ULIRGs with larger deviations from the $M_{\text{BH}} - \sigma$ line, they tend to have larger Eddington ratios and smaller BH masses. An evolutionary connection may exist between them. When the BH activity in ULIRGs is active enough, the central BH can blow away a large fraction of the surrounding gases, and the ULIRGs appear as Type I ULIRGs, their central BHs are still experiencing fast growth (i.e. with a large value of Eddington ratio), and they have relatively larger deviations from the typical $M_{\text{BH}} - \sigma$ relation. As the co-evolution of the central BH and its host galaxy, the host galaxy will form a spheroid gradually, and the growth of central BH becomes slower. At this time, the ULIRGs probably appear like optically bright QSOs. Thus the evolution of Type I ULIRGs is probably followed by the build up of $M_{\text{BH}} - \sigma$ relation and evolving towards the QSO phase.

Cao et al. (2008) compared the mid-infrared spectroscopic properties of 19 local Type I ULIRGs (named IR QSOs in their work) with that of QSOs and ULIRGs. They concluded that the MIR spectra slopes, the polycyclic aromatic hydrocarbon (PAH) emission strengths and [NeII] 12.81 μm luminosities of Type I ULIRGs differ from those of PG QSOs but are comparable with ULIRGs. Their results support that Type I ULIRGs are at a transitional stage from ULIRGs to classical QSOs, which are consistent with ours. Therefore, Type I ULIRGs are important for the understanding of co-evolution of the central BH and its host galaxy.

6. Conclusions

We identified 308 ULIRGs from the SDSS DR6 spectroscopy catalog and the IRAS faint source catalog. This is up to date the largest ULIRG sample with optical spectra in the local universe. About 56% of them show obvious interaction features, and this percentage increases for objects with smaller redshifts, probably due to the selection effect. After excluding the ULIRGs without obvious emission lines (with $S/N < 3$ or suffer serious absorptions around the emission lines), we got 147 NL ULIRGs (with only narrow emission lines in their spectra) and 62 Type I ULIRGs (with broad emission lines) in this sample. At least 49% of these 209 ULIRGs contains AGNs, and this percentage increases with L_{IR} . The ULIRGs near the Radio–FIR relation mainly have the starburst related emissions, and the radio excess in some objects is due to the AGN related radio emissions.

In combination with previous data, a large sample of 90 Type I ULIRGs is used to study their BH masses and black hole–host galaxy relation. We found that their BH masses are systematically smaller than those of PG QSOs, even the optical extinction effect were corrected through the Balmer decrement method. Their Eddington ratios are systematically larger than those of PG QSOs. Most Type I ULIRGs in our sample follow the $M_{\text{BH}} - \sigma$ relation, but some do not, even the FWHM of [OIII] narrow line core or [SII] was used as the surrogate of velocity dispersion, which implies that some Type I ULIRGs are in the early stage of galaxy evolution and their $M_{\text{BH}} - \sigma$ relation are still under building up.

We found an anti-correlation trend between $\log(M_{\text{BH}}/M_{\text{BHt}})$ and $\log(L_{\text{bol}}/L_{\text{Edd}})$, where M_{BHt} is the BH mass derived from the $M_{\text{BH}} - \sigma$ relation of Tremaine et al. (2002). The Type I ULIRGs with larger deviations from the $M_{\text{BH}} - \sigma$ relation tend to have larger Eddington ratios and smaller BH masses, and the ULIRGs which are close to the $M_{\text{BH}} - \sigma$ relation tend to have smaller Eddington ratios and larger BH masses. This anti-correlation trend implies that the evolution of Type I ULIRGs is probably followed by the build up of $M_{\text{BH}} - \sigma$ relation and evolving towards the QSO phase. Different types of ULIRGs are probably at different evolution stages.

We thank the referee for instructive comments, and Xiaoyang Xia, Fukun Liu, Hong Wu, Minzhi Kong, Ran Wang, Zhonglue Wen, Hui Shi, Zhaoyu Li for their helpful suggestions and discussions. This work is supported by the National Natural Science Foundation of China (0525313, 10521001, 10525113 and 10833003), and the National Key Basic Research Science Foundation of China (2007CB815403, 2007CB815405). Funding for the SDSS has been provided by the Alfred P. Sloan Foundation, the Participating Institutions, the National Science Foundation, the Department of Energy, the National Aeronautics and Space Administration, the Japanese Monbukagakusho, the Max Planck Society, and the Higher Education Funding

Council for England. The SDSS Web Site is <http://www.sdss.org>. The SDSS is managed by the Astrophysical Research Consortium for the Participating Institutions. The Participating Institutions are the American Museum of Natural History, Astrophysical Institute Potsdam, University of Basel, University of Cambridge, Case Western Reserve University, University of Chicago, Drexel University, Fermilab, the Institute for Advanced Study, the Japan Participation Group, Johns Hopkins University, the Joint Institute for Nuclear Astrophysics, the Kavli Institute for Particle Astrophysics and Cosmology, the Korean Scientist Group, the Chinese Academy of Sciences (LAMOST), Los Alamos National Laboratory, the Max Planck Institute for Astronomy (MPIA), the Max Planck Institute for Astrophysics (MPA), New Mexico State University, Ohio State University, University of Pittsburgh, University of Portsmouth, Princeton University, the United States Naval Observatory, and the University of Washington.

REFERENCES

- Adelman-McCarthy, J. K. et al. 2008, *ApJS*, 175, 297
- Alexander, D. M., Brandt, W. N., Smail, I., Swinbank, A. M., Bauer, F. E., Blain, A. W., Chapman, S. C., Coppin, K. E. K., Ivison, R. J., & Menéndez-Delmestre, K. 2008, *AJ*, 135, 1968
- Baldwin, J. A., Phillips, M. M., & Terlevich, R. 1981, *PASP*, 93, 5
- Becker, R. H., White, R. L., & Helfand, D. J. 1995, *ApJ*, 450, 559
- Best, P. N., Kauffmann, G., Heckman, T. M., & Ivezić, Ž. 2005, *MNRAS*, 362, 9
- Boroson, T. A. 2003, *ApJ*, 585, 647
- Boroson, T. A. & Green, R. F. 1992, *ApJS*, 80, 109
- Borys, C., Smail, I., Chapman, S. C., Blain, A. W., Alexander, D. M., & Ivison, R. J. 2005, *ApJ*, 635, 853
- Calzetti, D., Armus, L., Bohlin, R. C., Kinney, A. L., Koornneef, J., & Storchi-Bergmann, T. 2000, *ApJ*, 533, 682
- Canalizo, G. & Stockton, A. 2001, *ApJ*, 555, 719
- Cao, C., Wu, H., Wang, J.-L., Hao, C.-N., Deng, Z.-G., Xia, X.-Y., & Zou, Z.-L. 2006, *Chinese Journal of Astronomy and Astrophysics*, 6, 197

- Cao, C., Xia, X. Y., Wu, H., Mao, S., Hao, C. N., & Deng, Z. G. 2008, *MNRAS*, 390, 336
- Cardelli, J. A., Clayton, G. C., & Mathis, J. S. 1989, *ApJ*, 345, 245
- Clements, D. L., Sutherland, W. J., McMahon, R. G., & Saunders, W. 1996, *MNRAS*, 279, 477
- Colless, M., Dalton, G., Maddox, S., Sutherland, W., Norberg, P., Cole, S., Bland-Hawthorn, J., Bridges, T., Cannon, R., Collins, C., Couch, W., Cross, N., Deeley, K., De Propriis, R., Driver, S. P., Efsthathiou, G., Ellis, R. S., Frenk, C. S., Glazebrook, K., Jackson, C., Lahav, O., Lewis, I., Lumsden, S., Madgwick, D., Peacock, J. A., Peterson, B. A., Price, I., Seaborne, M., & Taylor, K. 2001, *MNRAS*, 328, 1039
- Condon, J. J., Anderson, M. L., & Helou, G. 1991a, *ApJ*, 376, 95
- Condon, J. J., Cotton, W. D., Greisen, E. W., Yin, Q. F., Perley, R. A., Taylor, G. B., & Broderick, J. J. 1998, *AJ*, 115, 1693
- Condon, J. J., Huang, Z.-P., Yin, Q. F., & Thuan, T. X. 1991b, *ApJ*, 378, 65
- Cui, J., Xia, X.-Y., Deng, Z.-G., Mao, S., & Zou, Z.-L. 2001, *AJ*, 122, 63
- Dasyra, K. M., Tacconi, L. J., Davies, R. I., Genzel, R., Lutz, D., Naab, T., Burkert, A., Veilleux, S., & Sanders, D. B. 2006a, *ApJ*, 638, 745
- Dasyra, K. M., Tacconi, L. J., Davies, R. I., Genzel, R., Lutz, D., Peterson, B. M., Veilleux, S., Baker, A. J., Schweitzer, M., & Sturm, E. 2007, *ApJ*, 657, 102
- Dasyra, K. M., Tacconi, L. J., Davies, R. I., Naab, T., Genzel, R., Lutz, D., Sturm, E., Baker, A. J., Veilleux, S., Sanders, D. B., & Burkert, A. 2006b, *ApJ*, 651, 835
- Dong, X., Wang, T., Wang, J., Yuan, W., Zhou, H., Dai, H., & Zhang, K. 2008, *MNRAS*, 383, 581
- Farrah, D., Rowan-Robinson, M., Oliver, S., Serjeant, S., Borne, K., Lawrence, A., Lucas, R. A., Bushouse, H., & Colina, L. 2001, *MNRAS*, 326, 1333
- Gao, Y. & Solomon, P. M. 2004, *ApJ*, 606, 271
- Goto, T. 2005, *MNRAS*, 360, 322
- Grupe, D. & Mathur, S. 2004, *ApJ*, 606, L41
- Hao, C. N., Xia, X. Y., Mao, S., Wu, H., & Deng, Z. G. 2005, *ApJ*, 625, 78

- Helou, G., Khan, I. R., Malek, L., & Boehmer, L. 1988, *ApJS*, 68, 151
- Helou, G., Soifer, B. T., & Rowan-Robinson, M. 1985, *ApJ*, 298, L7
- Hwang, H. S., Serjeant, S., Lee, M. G., Lee, K. H., & White, G. J. 2007, *MNRAS*, 375, 115
- Jones, D. H., Saunders, W., Colless, M., Read, M. A., Parker, Q. A., Watson, F. G., Campbell, L. A., Burkey, D., Mauch, T., Moore, L., Hartley, M., Cass, P., James, D., Russell, K., Fiegert, K., Dawe, J., Huchra, J., Jarrett, T., Lahav, O., Lucey, J., Mamon, G. A., Proust, D., Sadler, E. M., & Wakamatsu, K.-i. 2004, *MNRAS*, 355, 747
- Kaspi, S., Smith, P. S., Netzer, H., Maoz, D., Jannuzi, B. T., & Givon, U. 2000, *ApJ*, 533, 631
- Kauffmann, G., Heckman, T. M., Tremonti, C., Brinchmann, J., Charlot, S., White, S. D. M., Ridgway, S. E., Brinkmann, J., Fukugita, M., Hall, P. B., Ivezić, Ž., Richards, G. T., & Schneider, D. P. 2003, *MNRAS*, 346, 1055
- Kawakatu, N., Anabuki, N., Nagao, T., Umemura, M., & Nakagawa, T. 2006, *ApJ*, 637, 104
- Kewley, L. J., Groves, B., Kauffmann, G., & Heckman, T. 2006, *MNRAS*, 372, 961
- Kim, D.-C. & Sanders, D. B. 1998, *ApJS*, 119, 41
- Kim, D.-C., Veilleux, S., & Sanders, D. B. 1998, *ApJ*, 508, 627
- Komossa, S. & Xu, D. 2007, *ApJ*, 667, L33
- Lonsdale, C., Conrow, T., Evans, T., Fullmer, L., Moshir, M., Chester, T., Yentis, D., MacGillivray, H., Wolstencroft, R., & Egret, D. 1998, in *IAU Symposium*, Vol. 179, *New Horizons from Multi-Wavelength Sky Surveys*, ed. B. J. McLean, D. A. Golombek, J. J. E. Hayes, & H. E. Payne, 450–+
- Lonsdale, C. J., Farrah, D., & Smith, H. E. 2006, *Ultraluminous Infrared Galaxies (Astrophysics Update 2)*, 285–+
- Masci, F. J., Condon, J. J., Barlow, T. A., Lonsdale, C. J., Xu, C., Shupe, D. L., Pevunova, O., Fang, F., & Cutri, R. 2001, *PASP*, 113, 10
- McLure, R. J. & Jarvis, M. J. 2002, *MNRAS*, 337, 109
- Mirabel, I. F. & Sanders, D. B. 1988, *ApJ*, 335, 104

- Moshir, M., Kopman, G., & Conrow, T. A. O. 1992, IRAS Faint Source Survey, Explanatory supplement version 2 (Pasadena: Infrared Processing and Analysis Center, California Institute of Technology, 1992, edited by Moshir, M.; Kopman, G.; Conrow, T. a.o.)
- Murphy, Jr., T. W., Armus, L., Matthews, K., Soifer, B. T., Mazzarella, J. M., Shupe, D. L., Strauss, M. A., & Neugebauer, G. 1996, *AJ*, 111, 1025
- Nelson, C. H. 2000, *ApJ*, 544, L91
- Pasquali, A., Kauffmann, G., & Heckman, T. M. 2005, *MNRAS*, 361, 1121
- Peterson, B. M. & Wandel, A. 1999, *ApJ*, 521, L95
- . 2000, *ApJ*, 540, L13
- Roy, A. L. & Norris, R. P. 1997, *MNRAS*, 289, 824
- Salviander, S., Shields, G. A., Gebhardt, K., & Bonning, E. W. 2007, *ApJ*, 662, 131
- Sanders, D. B., Mazzarella, J. M., Kim, D.-C., Surace, J. A., & Soifer, B. T. 2003, *AJ*, 126, 1607
- Sanders, D. B. & Mirabel, I. F. 1996, *ARA&A*, 34, 749
- Sanders, D. B., Scoville, N. Z., & Soifer, B. T. 1991, *ApJ*, 370, 158
- Sanders, D. B., Scoville, N. Z., Young, J. S., Soifer, B. T., Schloerb, F. P., Rice, W. L., & Danielson, G. E. 1986, *ApJ*, 305, L45
- Soifer, B. T., Sanders, D. B., Madore, B. F., Neugebauer, G., Danielson, G. E., Elias, J. H., Lonsdale, C. J., & Rice, W. L. 1987, *ApJ*, 320, 238
- Stanford, S. A., Stern, D., van Breugel, W., & De Breuck, C. 2000, *ApJS*, 131, 185
- Strauss, M. A., Davis, M., Yahil, A., & Huchra, J. P. 1990, *ApJ*, 361, 49
- Surace, J. A., Sanders, D. B., & Evans, A. S. 2000, *ApJ*, 529, 170
- Sutherland, W. & Saunders, W. 1992, *MNRAS*, 259, 413
- Tremaine, S., Gebhardt, K., Bender, R., Bower, G., Dressler, A., Faber, S. M., Filippenko, A. V., Green, R., Grillmair, C., Ho, L. C., Kormendy, J., Lauer, T. R., Magorrian, J., Pinkney, J., & Richstone, D. 2002, *ApJ*, 574, 740
- Veilleux, S., Kim, D.-C., & Sanders, D. B. 1999a, *ApJ*, 522, 113

- . 2002, *ApJS*, 143, 315
- Veilleux, S., Kim, D.-C., Sanders, D. B., Mazzarella, J. M., & Soifer, B. T. 1995, *ApJS*, 98, 171
- Veilleux, S., Sanders, D. B., & Kim, D.-C. 1997, *ApJ*, 484, 92
- . 1999b, *ApJ*, 522, 139
- White, R. L., Becker, R. H., Helfand, D. J., & Gregg, M. D. 1997, *ApJ*, 475, 479
- Wu, H., Zou, Z. L., Xia, X. Y., & Deng, Z. G. 1998a, *A&AS*, 127, 521
- . 1998b, *A&AS*, 132, 181
- Yun, M. S., Reddy, N. A., & Condon, J. J. 2001, *ApJ*, 554, 803
- Zheng, X. Z., Xia, X. Y., Mao, S., Wu, H., & Deng, Z. G. 2002, *AJ*, 124, 18
- Zheng, Z., Wu, H., Mao, S., Xia, X.-Y., Deng, Z.-G., & Zou, Z.-L. 1999, *A&A*, 349, 735
- Zou, Z., Xia, X., Deng, Z., & Su, H. 1991, *MNRAS*, 252, 593

A. The parameters of our samples (online version)

Table 1. The parameters of our ULIRG sample.

IRAS name	z_{sdss}	SDSS name	$\log(\frac{L_{\text{FIR}}}{L_{\odot}})$	$S_{\text{NVSS}}^{\text{1.4GHz}}$ (mJy)	$S_{\text{FIRST}}^{\text{1.4GHz}}$ (mJy)	Note	NED	$f_{\text{H}\beta}$	$f_{\text{OIII}5007}$	$f_{\text{H}\alpha}$	$f_{\text{NII}6583}$	f_{SII}	$f_{\text{OI}6300}$	Note
(1)	(2)	(3)	(4)	(5)	(6)	(7)	(8)	(9)	(10)	(11)	(12)	(13)	(14)	(15)
F00090−0054	0.195	J001138.79−003813.7	12.10		1.17	I	Yes							
F01093−1002	0.131	J011152.64−094559.8	12.00	6.2	5.38	n	Yes	0.92±0.07	0.61±0.04	6.02±0.07	3.54±0.06	2.45±0.10	0.46±0.03	Composite
F01166−0844	0.118	J011907.57−082909.6	12.09		2.10	III	Yes	0.73±0.04	0.15±0.03	3.11±0.06	1.67±0.04	1.02±0.04	0.06±0.02	Starburst
F01329+1439	0.218	J013537.56+145510.9	12.17			n	Yes	6.14±0.06	13.51±0.09	26.22±0.16	5.03±0.06	6.22±0.07	0.87±0.03	Starburst
F01347+0042	0.198	J013720.02+005722.3	12.10	3.3	2.92	III	Yes	0.32±0.10	0.20±0.04	2.92±0.08	2.05±0.07	1.37±0.07	0.25±0.04	Composite
F01462+0014	0.280	J014852.58+002859.9	12.31	2.8	2.38	II	Yes	0.92±0.04	0.76±0.03	6.70±0.10	3.82±0.09	2.27±0.08	0.33±0.05	Composite
F01478+1254	0.147	J015028.40+130858.4	12.02			III	Yes	7.45±0.13	17.94±0.09	28.73±0.13	6.30±0.04	6.21±0.05	0.81±0.03	Starburst
F01572+0009	0.163	J015950.25+002340.8	12.52	26.2	24.08	I	Yes							
F02016−0108	0.334	J020412.43−005351.4	12.63			n	Yes							
F02280−0746	0.295	J023028.69−073304.5	12.20		1.27	n	Yes	0.53±0.05	0.37±0.03	4.56±0.09	2.80±0.06	2.08±0.08	0.19±0.04	Composite
F02417−0043	0.200	J024417.44−003041.1	12.14	10.3	9.39	III	Yes	0.64±0.05	5.77±0.46	8.43±0.14	15.63±0.15	4.50±0.09	0.97±0.06	Seyfert
F02486−0714	0.327	J025105.28−070230.2	12.32	6.9	5.80	I	Yes							
F03209−0806	0.166	J032322.87−075615.3	12.27	4.8		I	Yes	0.94±0.04	0.91±0.05	9.24±0.07	6.92±0.06	3.26±0.06	0.58±0.04	Composite
F03264−0705	0.220	J032855.39−065535.8	12.04			II	No							
F07391+3219	0.380	J074217.08+321315.1	12.67			II	Yes							
F07445+2435	0.208	J074737.14+242802.6	12.15		1.35	n	No							
F07448+1813	0.340	J074741.95+180528.1	12.46			n	No							
F07460+1728	0.167	J074855.47+172125.5	12.02			III	No							
F07479+2646	0.384	J075104.19+263850.9	12.49		1.62	I	Yes							
F07526+4858	0.349	J075622.12+484941.8	12.47			n	Yes							
F07548+4227	0.211	J075819.69+421935.1	12.13	3.4	1.81	II	Yes							
F07561+2441	0.227	J075904.49+243307.7	12.08	2.5		II	No							
F07578+5148	0.196	J080142.16+514023.4	12.07			n	No							
F07592+3736	0.238	J080234.13+372801.3	12.14		3.36	III	Yes	1.78±0.07	6.91±0.07	12.22±0.12	9.84±0.10	6.89±0.10	1.53±0.06	Seyfert
F08028+3310	0.246	J080601.71+330157.6	12.22		1.93	n	No	0.85±0.04	2.61±0.05	7.87±0.10	4.78±0.08	2.12±0.09	0.47±0.06	Ambiguity
F08030+5243	0.083	J080650.80+523507.3	12.08	15.3	15.36	n	Yes	1.91±0.05	1.60±0.06	24.10±0.17	12.03±0.11	7.73±0.11	1.10±0.05	Composite
F08031+1729	0.209	J080559.47+172119.8	12.42			I	No							
F08050+3909	0.368	J080824.75+390016.2	12.80			n	No							
F08072+1622	0.186	J081005.28+161345.7	12.15		2.14	n	Yes	1.83±0.04	6.08±0.06	12.18±0.11	7.90±0.08	3.39±0.08	0.37±0.04	Ambiguity
F08079+2822	0.350	J081107.06+281316.1	12.47			n	Yes							
F08091+3449	0.256	J081227.65+344100.9	12.39		2.98	n	Yes	0.39±0.13	6.73±0.16	3.82±0.08	4.97±0.10	2.48±0.10	0.57±0.06	Seyfert

Table 1—Continued

IRAS name	z_{sdss}	SDSS name	$\log(\frac{L_{\text{FIR}}}{L_{\odot}})$	$S_{1.4\text{GHz}}^{\text{SNVSS}}$ (mJy)	$S_{1.4\text{GHz}}^{\text{FIRST}}$ (mJy)	Note	NED	$f_{\text{H}\beta}$	$f_{\text{OIII}5007}$	$f_{\text{H}\alpha}$	$f_{\text{NII}6583}$	f_{SII}	$f_{\text{OI}6300}$	Note
(1)	(2)	(3)	(4)	(5)	(6)	(7)	(8)	(9)	(10)	(11)	(12)	(13)	(14)	(15)
F08162+2716	0.261	J081916.24+270729.7	12.52	6.7		n	Yes	0.13±0.03	1.77±0.03	0.92±0.06	0.58±0.07	0.45±0.06		Seyfert
F08180+5612	0.159	J082203.51+560301.2	12.08	12.1	12.31	I	No	1.10±0.60	8.46±0.27	9.10±0.13	7.71±0.09	5.49±0.07	1.55±0.05	Seyfert
F08197+4519	0.264	J082317.24+451009.1	12.43		1.15	I	Yes	0.19±0.02	0.26±0.02	2.38±0.05	1.41±0.03	0.95±0.05	0.19±0.03	Composite
F08201+2801	0.168	J082312.61+275139.8	12.30	16.3	4.74	I	Yes	1.01±0.04	1.01±0.04	7.83±0.07	3.82±0.05	3.08±0.06	0.52±0.04	Composite
F08209+2458	0.234	J082355.36+244830.4	12.19		0.94	n	Yes							
F08219+1549	0.220	J082445.63+153944.1	12.15	5.3	3.11	I	Yes	0.27±0.10	1.76±0.06	3.21±0.08	4.43±0.09	1.52±0.08	0.27±0.04	Seyfert
F08220+3842	0.206	J082521.65+383258.6	12.09	3.4	2.36	II	Yes							
F08238+0752	0.311	J082633.51+074248.4	12.41			n	Yes							
F08252+4632	0.281	J082848.16+462229.2	12.35	2.2	1.29	n	Yes	0.21±0.04	0.34±0.02	1.77±0.05	1.47±0.06	0.62±0.06	0.20±0.03	Ambiguity
F08266+3855	0.196	J082951.21+384522.0	12.09	2.8	2.53	III	Yes							
F08274+1930	0.186	J083019.75+192050.0	12.11			I	No	3.32±0.04	2.99±0.04	14.85±0.09	5.58±0.05	3.69±0.07	0.37±0.03	Starburst
F08297+4728	0.299	J083312.44+471817.8	12.38		1.70	I	Yes	0.44±0.02	1.12±0.03	3.18±0.05	2.39±0.06	1.58±0.07	0.29±0.04	Seyfert
F08313+4855	0.175	J083457.66+484515.6	12.21	8.2	7.88	I	No							
F08322+3609	0.201	J083527.48+355932.6	12.03		0.85	I	Yes	0.35±0.04	0.57±0.03	2.98±0.06	1.96±0.06	0.82±0.05	0.21±0.04	Composite
F08344+5105	0.097	J083803.61+505508.8	12.05	8.3	7.53	I	Yes	0.78±0.05	0.84±0.04	8.75±0.08	4.71±0.06	3.49±0.08	0.61±0.04	Composite
F08382+3707	0.228	J084127.71+365616.7	12.00		1.35	n	Yes							
F08407+2630	0.257	J084349.75+261910.8	12.10			n	Yes							
F08435+3141	0.386	J084634.31+313058.2	12.46			n	No							
F08438+3150	0.387	J084657.52+313916.2	12.62	7.1	5.12	n	Yes							
F08449+2332	0.152	J084750.18+232108.7	12.09	5.8	3.24	III	Yes	0.63±0.06	0.74±0.07	3.66±0.07	1.86±0.06	1.49±0.07	0.23±0.06	Composite
F08451+3651	0.170	J084821.35+364039.7	12.01	5.0	4.93	II	Yes							
F08499+0145	0.195	J085233.93+013422.9	12.07			II	Yes	1.65±0.04	2.20±0.04	7.44±0.06	2.00±0.05	2.08±0.06	0.25±0.03	Starburst
F08504+0705	0.483	J085304.26+065403.0	12.95		0.94	n	Yes							
F08504+2538	0.256	J085325.07+252656.0	12.38		10.46	n	No							
F08507+3636	0.261	J085356.80+362456.0	12.22	33.8	16.16	II	Yes	0.51±0.20	4.46±0.31	5.40±0.11	7.49±0.13	4.10±0.09	0.80±0.06	Seyfert
F08526+3720	0.357	J085554.47+370900.5	12.50		0.90	I	Yes	0.73±0.59	7.40±0.36	3.94±0.12	2.48±0.10	0.96±0.10	0.42±0.06	Seyfert
F08542+1920	0.331	J085706.35+190853.5	12.46	4.4	4.43	n	Yes							
F08572+3915	0.058	J090025.37+390353.7	12.04	4.3	4.89	II	Yes	1.18±0.04	1.65±0.05	10.96±0.10	4.51±0.06	4.67±0.06	0.69±0.03	Composite
F08591+5248	0.157	J090248.90+523624.6	12.21	7.7	5.96	n	Yes	1.52±0.22	0.77±0.07	9.26±0.11	7.34±0.09	3.71±0.08	0.76±0.05	Composite
F09005+0223	0.329	J090307.84+021152.2	12.56	24.2	22.50	n	Yes							
F09005+2253	0.290	J090325.62+224147.5	12.24		0.84	n	Yes							

Table 1—Continued

IRAS name	z_{sdss}	SDSS name	$\log(\frac{L_{\text{FIR}}}{L_{\odot}})$	SNVSS 1.4GHz (mJy)	SFIRST 1.4GHz (mJy)	Note	NED	$f_{\text{H}\beta}$	$f_{\text{OIII}5007}$	$f_{\text{H}\alpha}$	$f_{\text{NII}6583}$	f_{SII}	$f_{\text{OI}6300}$	Note
(1)	(2)	(3)	(4)	(5)	(6)	(7)	(8)	(9)	(10)	(11)	(12)	(13)	(14)	(15)
F09008+3643	0.288	J090359.91+363054.7	12.55		2.05	n	Yes							
F09025+1253	0.196	J090517.05+124151.9	12.17	4.2		II	No							
F09029+2430	0.232	J090554.71+241828.8	12.15	3.9	3.48	II	No	0.07±0.03	0.78±0.05	2.35±0.08	3.62±0.09	2.15±0.10	0.52±0.06	Seyfert
F09036+2706	0.341	J090633.96+265419.6	12.39		1.44	n	No	0.95±0.05	3.72±0.04	5.39±0.10	1.82±0.15	0.97±0.09	0.23±0.03	Ambiguity
F09039+0503	0.125	J090634.04+045127.6	12.14	6.2	4.92	I	Yes	1.63±0.06	1.42±0.06	11.71±0.11	10.50±0.10	6.72±0.08	1.43±0.05	Composite
F09045+3943	0.224	J090742.25+393149.8	12.02		1.24	I	Yes	0.82±0.04	1.15±0.03	4.17±0.06	1.56±0.05	1.60±0.06	0.28±0.04	Composite
F09083+0311	0.504	J091050.01+025939.6	13.00	6.1	4.26	n	Yes							
F09097+5342	0.254	J091319.02+532958.5	12.07		0.87	III	No	0.32±0.04	1.20±0.05	3.48±0.09	3.87±0.08	1.96±0.08	0.34±0.04	Seyfert
F09105+4108	0.442	J091345.49+405628.2	12.87	15.9	8.27	I	Yes							
F09116+0334	0.145	J091413.79+032201.3	12.18	10.5	9.41	I	Yes	1.48±0.45	0.72±0.08	12.11±0.14	11.67±0.13	4.44±0.12	0.71±0.07	Composite
F09119+0945	0.246	J091438.14+093322.9	12.31		1.18	II	Yes	0.48±0.03	0.40±0.03	3.47±0.05	3.19±0.05	1.02±0.06	0.24±0.06	Composite
F09186+4521	0.235	J092159.39+450912.4	12.04			n	No	1.97±0.06	1.91±0.06	10.89±0.11	5.56±0.08	2.99±0.09	0.62±0.05	Composite
F09198+0323	0.174	J092226.71+031048.2	12.05	2.2		II	Yes							
F09217+5348	0.195	J092518.47+533525.0	12.04		1.20	I	No	0.24±0.11	0.18±0.03	1.18±0.04	1.39±0.05	0.93±0.05	0.22±0.03	LINERs
F09220+2759	0.531	J092501.79+274608.0	12.92	26.3	26.74	n	No							
F09240+4804	0.237	J092723.13+475147.3	12.07			II	No	1.12±0.03	0.54±0.03	6.48±0.06	2.94±0.05	1.56±0.06		Starburst
F09246+0115	0.169	J092710.88+010232.2	12.07		2.66	I	Yes	1.32±0.05	0.61±0.05	10.75±0.08	5.00±0.05	3.28±0.08	0.46±0.04	Starburst
F09258+1735	0.252	J092838.64+172220.4	12.16	5.6	5.76	n	No							
F09306+5431	0.232	J093402.47+541751.5	12.17			III	Yes							
F09320+6134	0.039	J093551.61+612111.4	12.02	170.1	146.74	I	Yes	1.29±0.07	2.56±0.07	22.31±0.17	29.70±0.18	9.19±0.12	1.60±0.07	Ambiguity
F09322+0432	0.198	J093451.87+041848.2	12.13	3.0	1.41	II	Yes							
F09323+6222	0.225	J093613.72+620905.4	12.06			I	No							
F09395+3939	0.194	J094239.17+392559.7	12.14	3.5	3.53	II	Yes	0.45±0.05	0.57±0.06	6.24±0.08	3.62±0.09	1.96±0.09	0.37±0.05	Composite
F09398+0013	0.146	J094224.28−000005.0	12.06	5.5	4.87	I	Yes	0.83±0.04	1.67±0.05	10.26±0.08	5.52±0.06	4.48±0.07	0.79±0.04	Composite
F09437+1720	0.243	J094635.73+170558.4	12.02		1.97	n	No	2.30±0.04	1.49±0.04	11.55±0.11	5.62±0.07	3.81±0.10	0.75±0.05	Composite
F09438+4735	0.539	J094704.52+472143.0	13.01	3.1	2.84	n	Yes							
F09444+1019	0.202	J094706.99+100611.6	12.01		1.97	I	No	1.59±0.06	1.47±0.05	9.29±0.10	3.77±0.08	3.10±0.07	0.58±0.04	Composite Starburst
F09469+6234	0.213	J095047.39+622021.3	12.00			n	No							
F09501+5535	0.324	J095331.87+552102.2	12.54	2.5	1.07	n	Yes							
F09555+5109	0.215	J095846.85+505456.5	12.18			II	No	0.47±0.11	1.39±0.04	3.50±0.08	1.95±0.07	1.25±0.06	0.16±0.04	Seyfert
F09583+4714	0.086	J100131.21+465946.8	12.02		24.95	II	Yes	3.05±0.64	11.21±0.52	62.91±0.21	25.23±0.96	13.98±0.11	5.09±0.07	Composite

Table 1—Continued

IRAS name	z_{sdss}	SDSS name	$\log(\frac{L_{\text{FIR}}}{L_{\odot}})$	SNVSS 1.4GHz (mJy)	SFIRST 1.4GHz (mJy)	Note	NED	$f_{\text{H}\beta}$	$f_{\text{OIII}5007}$	$f_{\text{H}\alpha}$	$f_{\text{NII}6583}$	f_{SII}	$f_{\text{OI}6300}$	Note
(1)	(2)	(3)	(4)	(5)	(6)	(7)	(8)	(9)	(10)	(11)	(12)	(13)	(14)	(15)
F09591+2045	0.357	J100153.66+203141.1	12.50		1.35	I	No							
F10015−0018	0.289	J100404.99−003253.4	12.52	4.0	2.55	I	Yes							
F10017+4011	0.312	J100445.17+395732.3	12.27		1.61	n	Yes							
F10022+5233	0.226	J100539.16+521842.7	12.05			n	No							
F10026+3107	0.235	J100532.13+305318.2	12.03	2.5	3.62	n	Yes							
F10026+4347	0.179	J100541.86+433240.3	12.08		2.81	n	Yes							
F10026−0022	0.407	J100513.11−003721.4	12.66			n	No							
F10030+4126	0.328	J100603.85+411224.8	12.49		2.21	n	Yes	0.86±0.03	1.57±0.04	5.23±0.10	1.60±0.08	1.94±0.18		Starburst
F10035+2740	0.166	J100626.33+272546.4	12.30	5.8	5.44	I	Yes	0.32±0.04	0.66±0.05	2.72±0.06	2.91±0.05	2.46±0.06	0.52±0.04	LINERs
F10035+4852	0.065	J100645.86+483743.8	12.03	28.1	8.59	II	Yes	1.00±0.05	0.41±0.04	7.81±0.08	3.97±0.06	3.04±0.06	0.35±0.03	Composite
F10037+1112	0.274	J100624.37+105748.4	12.15		1.15	n	Yes	1.58±0.04	4.06±0.05	8.05±0.09	2.22±0.06	2.27±0.08	0.37±0.04	Composite
F10040+0932	0.171	J100643.50+091727.5	12.22	3.0	2.58	n	Yes	1.16±0.07	0.86±0.05	7.28±0.07	3.87±0.07	2.37±0.07	0.35±0.04	Composite
F10052+2959	0.257	J100809.48+294425.9	12.11	2.6	1.66	n	Yes	0.22±0.10	0.49±0.06	2.51±0.08	3.05±0.10	0.87±0.10		Ambiguity
F10059+3605	0.161	J100852.90+355103.0	12.03			n	No							
F10105+6118	0.213	J101358.92+610431.9	12.01		0.85	I	No	1.17±0.07	1.49±0.04	5.64±0.08	2.41±0.06	1.85±0.06	0.33±0.04	Composite
F10106+2227	0.274	J101325.42+221229.4	12.15		1.08	n	No							
F10107+4708	0.206	J101348.08+465359.5	12.34		2.15	I	No							
F10124+2742	0.210	J101515.35+272717.1	12.24	5.6	5.36	n	No	1.68±0.07	4.24±0.07	12.70±0.11	9.16±0.09	5.13±0.07	0.91±0.07	Seyfert
F10190+1322	0.076	J102142.79+130656.1	12.07	16.8	16.41	II	Yes							
F10194+2427	0.188	J102212.64+241202.4	12.04	3.9	4.08	I	No	0.51±0.15	1.17±0.05	4.17±0.08	3.30±0.07	1.55±0.07	0.29±0.04	Ambiguity
F10196+3707	0.267	J102229.18+365209.7	12.20		1.42	III	No	1.62±0.04	1.53±0.03	9.02±0.09	4.11±0.09	2.70±0.07	0.42±0.04	Composite
F10211+2436	0.209	J102359.20+242106.3	12.06			I	No	6.07±0.06	16.62±0.09	23.63±0.16	4.92±0.07	4.41±0.06	0.67±0.04	Starburst
F10212+2506	0.196	J102403.67+245139.3	12.11	2.6	1.87	I	Yes							
F10234+3052	0.340	J102617.48+303643.1	12.47	3.4	1.82	n	Yes							
F10253+0854	0.417	J102755.84+083913.3	12.65			II	Yes							
F10341+1312	0.174	J103650.91+125714.7	12.06	4.9	3.16	n	Yes							
F10345+3809	0.203	J103728.97+375407.6	12.05			I	No	2.41±0.06	4.22±0.05	11.76±0.11	2.30±0.07	3.79±0.07	0.52±0.04	Starburst
F10360+1428	0.375	J103840.87+141307.5	12.51			II	Yes							
F10369+4913	0.175	J104000.53+485744.5	12.06	7.5	7.25	I	Yes	3.01±0.06	2.07±0.07	15.34±0.13	7.65±0.08	5.14±0.09	0.84±0.05	Composite
F10372+4801	0.486	J104014.42+474554.7	12.81	4.1	4.28	n	Yes							
F10378+1108	0.136	J104029.17+105318.3	12.34	8.4	8.55	I	Yes	1.30±0.28	2.75±0.35	13.63±0.13	15.42±0.13	8.66±0.12	2.08±0.06	LINERs

Table 1—Continued

IRAS name	z_{sdss}	SDSS name	$\log(\frac{L_{\text{FIR}}}{L_{\odot}})$	SNVSS 1.4GHz (mJy)	SFIRST 1.4GHz (mJy)	Note	NED	$f_{\text{H}\beta}$	$f_{\text{OIII}5007}$	$f_{\text{H}\alpha}$	$f_{\text{NII}6583}$	f_{SII}	$f_{\text{OI}6300}$	Note
(1)	(2)	(3)	(4)	(5)	(6)	(7)	(8)	(9)	(10)	(11)	(12)	(13)	(14)	(15)
F10418+1153	0.230	J104429.27+113811.3	12.06	190.4	26.69	I	Yes	0.23±0.06	3.65±0.06	2.16±0.06	3.02±0.07	0.97±0.07	0.42±0.06	Seyfert
F10445+4205	0.199	J104726.60+414956.7	12.14		1.00	II	Yes	1.16±0.05	1.15±0.04	7.82±0.08	3.30±0.05	2.64±0.06	0.36±0.03	Composite
F10494+4424	0.092	J105223.52+440847.6	12.25	21.2	20.74	I	Yes	0.42±0.06	0.69±0.05	5.95±0.07	4.67±0.06	3.00±0.07	0.68±0.04	Composite
F10507+3329	0.243	J105330.94+331342.3	12.05		2.69	I	Yes	0.35±0.05	0.67±0.04	2.84±0.06	2.90±0.06	0.85±0.07	0.17±0.04	Ambiguity
F10522+0003	0.220	J105447.31−001227.7	12.24	2.9	1.82	II	Yes							
F10531+5531	0.256	J105609.81+551604.2	12.01			I	No							
F10538+3309	0.457	J105633.12+325337.7	12.62			n	No							
F10544+6123	0.257	J105736.77+610737.2	12.08			I	No	0.75±0.04	0.26±0.02	3.15±0.04	1.40±0.04	0.87±0.05	0.15±0.05	Starburst
F10558+3845	0.208	J105839.30+382906.6	12.23		2.25	I	Yes	0.40±0.09	0.26±0.03	2.58±0.06	1.63±0.06	0.89±0.06	0.15±0.05	Composite
F10594+3818	0.158	J110214.00+380234.6	12.31	9.7	9.61	I	Yes	3.40±0.08	2.30±0.08	21.37±0.20	11.73±0.13	7.03±0.10	0.92±0.05	Composite
F11028+3130	0.199	J110537.54+311432.2	12.43		2.27	I	Yes							
F11028+3442	0.509	J110539.82+342534.6	12.86			n	Yes							
F11057+4053	0.165	J110832.95+403731.7	12.08	4.7	3.90	I	Yes	0.28±0.08	0.51±0.07	3.79±0.09	4.87±0.08	1.78±0.08	0.49±0.06	Ambiguity
F11062+0715	0.181	J110851.03+065901.4	12.01	11.1	9.84	I	No	4.90±0.09	30.54±0.40	38.80±0.29	10.31±0.36	13.71±0.13	3.31±0.14	Seyfert
F11066+4242	0.232	J110926.71+422558.1	12.11	2.4	1.73	I	No							
F11070+4249	0.261	J110952.83+423315.7	12.34	15.4	16.96	n	Yes							
F11087+5351	0.143	J111136.37+533459.4	12.03	31.9	30.97	I	Yes	0.75±0.04	3.07±0.07	6.96±0.09	7.00±0.08	4.85±0.06	1.18±0.04	Seyfert
F11095+2749	0.235	J111211.07+273256.2	12.15	3.5	2.56	I	Yes	5.78±0.06	12.78±0.11	27.29±0.21	6.54±0.08	7.05±0.11	1.14±0.05	Starburst
F11134+0225	0.211	J111603.13+020852.2	12.01		0.57	n	Yes							
F11162+6020	0.264	J111907.01+600430.8	12.55	44.5	56.22	I	Yes							
F11163+3207	0.261	J111902.27+315122.6	12.22	36.1	34.38	n	Yes							
F11188+1138	0.185	J112129.00+112225.7	12.35	7.1	6.53	I	Yes	1.43±0.09	5.73±0.07	12.56±0.11	11.47±0.11	4.13±0.09	0.88±0.05	Seyfert
F11206+3639	0.242	J112319.19+362331.1	12.42	22.5	13.54	I	No							
F11213+6556	0.264	J112424.60+653945.8	12.28			I	Yes							
F11215+1058	0.199	J112409.72+104201.8	12.08		1.38	III	No	0.43±0.05	0.84±0.06	4.61±0.08	4.56±0.08	1.90±0.08	0.33±0.05	Ambiguity
F11215+3853	0.295	J112414.54+383650.9	12.31		1.94	n	Yes							
F11307+0449	0.248	J113320.91+043255.2	12.12	3.4	5.02	n	No							
F11327+4137	0.183	J113524.86+412119.8	12.00			n	No							
F11364+1307	0.235	J113901.98+125117.7	12.18			I	Yes							
F11370+4647	0.173	J113939.35+463132.1	12.06	4.4	4.95	I	No							
F11387+4116	0.149	J114122.03+405950.3	12.15	6.5	5.39	n	Yes	0.59±0.14	0.32±0.05	5.49±0.08	5.12±0.08	2.12±0.08	0.36±0.06	Composite

Table 1—Continued

IRAS name	z_{sdss}	SDSS name	$\log(\frac{L_{\text{FIR}}}{L_{\odot}})$	$S_{1.4\text{GHz}}^{\text{NVSS}}$ (mJy)	$S_{1.4\text{GHz}}^{\text{FIRST}}$ (mJy)	Note	NED	$f_{\text{H}\beta}$	$f_{\text{OIII}5007}$	$f_{\text{H}\alpha}$	$f_{\text{NII}6583}$	f_{SII}	$f_{\text{OI}6300}$	Note
(1)	(2)	(3)	(4)	(5)	(6)	(7)	(8)	(9)	(10)	(11)	(12)	(13)	(14)	(15)
F11394+0108	0.245	J114203.41+005135.9	12.22	19.2	17.68	I	Yes							
F11417+1151	0.271	J114420.31+113500.8	12.33		2.62	n	No							
F11506+1331	0.127	J115314.23+131427.9	12.39	13.5	13.16	I	Yes	0.86±0.04	1.55±0.05	10.23±0.09	4.37±0.06	4.23±0.07	0.97±0.04	Composite
F11514+1212	0.365	J115402.70+115528.4	12.62			n	Yes							
F11518+2746	0.267	J115420.94+273001.6	12.17			III	No							
F11553−0259	0.215	J115753.20−031537.1	12.06	3.3	2.58	n	Yes							
F11557+1342	0.439	J115816.72+132624.2	12.66		2.47	n	No							
F11595+1144	0.194	J120205.59+112812.2	12.34	8.7	5.77	n	Yes	3.01±0.08	3.46±0.07	19.10±0.15	8.37±0.11	5.96±0.10	0.87±0.06	Composite
F12043+5215	0.398	J120652.44+515918.7	12.51		1.32	n	Yes							
F12047+0233	0.221	J120721.45+021657.7	12.13		1.74	n	Yes	0.98±0.05	0.84±0.03	7.00±0.07	4.31±0.05	1.96±0.05	0.29±0.03	Composite
F12112+0305	0.073	J121346.07+024841.5	12.38	23.3	24.64	II	Yes	1.31±0.04	3.24±0.05	13.74±0.09	6.92±0.06	6.82±0.06	1.55±0.04	Composite
F12126+0943	0.263	J121509.84+092709.5	12.09			I	Yes	0.22±0.36	0.41±0.04	1.27±0.12	1.81±0.08	1.55±0.10	0.35±0.07	LINERs
F12136+3919	0.334	J121608.15+390245.7	12.70	2.7		n	No							
F12232+5532	0.232	J122538.31+551548.9	12.36	3.6	4.96	n	Yes	0.50±0.08	0.71±0.05	3.56±0.08	1.86±0.07	1.94±0.12		Composite
F12288+2811	0.212	J123121.37+275524.0	12.08	2.4	1.30	I	No							
F12297+5222	0.391	J123205.48+520613.4	12.61	3.8	4.12	n	Yes							
F12375+3721	0.238	J123959.05+370505.1	12.11	7.9	6.13	III	No							
F12433+6540	0.320	J124526.98+652358.3	12.36			n	Yes							
F12442+4550	0.196	J124633.52+453421.7	12.28		2.77	III	Yes							
F12447+3721	0.158	J124707.75+370536.7	12.14	2.7	2.17	I	Yes	6.99±0.08	17.45±0.13	29.96±0.22	5.85±0.08	7.83±0.08	1.28±0.04	Ambiguity
F12465+4458	0.228	J124854.99+444213.8	12.09			II	No	0.99±0.05	9.53±0.09	4.67±0.08	2.76±0.06	1.88±0.07	0.38±0.04	Seyfert
F12469+4359	0.302	J124916.55+434254.6	12.36		1.81	n	Yes	0.63±0.04	0.58±0.04	5.30±0.10	2.98±0.08	2.29±0.14	0.49±0.07	Composite
F12471+4759	0.304	J124927.86+474249.7	12.55	3.2	2.53	n	Yes							
F12482+3135	0.264	J125037.03+311853.0	12.14			n	No							
F12487+0235	0.253	J125120.04+021902.4	12.37		2.22	I	Yes	0.27±0.04	0.34±0.04	3.57±0.07	3.39±0.07	1.72±0.10	0.23±0.06	Ambiguity
F12489+6619	0.282	J125100.45+660326.8	12.17			n	Yes							
F12494+3227	0.326	J125154.92+321110.5	12.41	2.7	1.16	I	Yes							
F12532−0322	0.169	J125547.83−033909.6	12.06	3.4	3.74	I	Yes	1.62±0.06	7.83±0.09	11.55±0.09	7.95±0.07	4.88±0.08	0.96±0.05	Seyfert
F12535+0254	0.219	J125604.92+023831.9	12.26			n	Yes							
F12563+3640	0.362	J125839.02+362449.8	12.51			n	No							
F13005+6343	0.335	J130236.96+632656.2	12.37			I	Yes							

Table 1—Continued

IRAS name	z_{sdss}	SDSS name	$\log(\frac{L_{\text{FIR}}}{L_{\odot}})$	SNVSS 1.4GHz (mJy)	SFIRST 1.4GHz (mJy)	Note	NED	$f_{\text{H}\beta}$	$f_{\text{OIII}5007}$	$f_{\text{H}\alpha}$	$f_{\text{NII}6583}$	f_{SII}	$f_{\text{OI}6300}$	Note
(1)	(2)	(3)	(4)	(5)	(6)	(7)	(8)	(9)	(10)	(11)	(12)	(13)	(14)	(15)
F13096+4507	0.232	J131201.62+445109.9	12.20			n	No							
F13161+0927	0.282	J131842.18+091112.9	12.22		0.99	I	No	0.89±0.06	2.82±0.05	7.34±0.09	6.99±0.10	2.57±0.10	0.59±0.05	Seyfert
F13163+5237	0.355	J131827.08+522049.8	12.66			n	No							
F13190+4050	0.185	J132117.48+403519.5	12.08	2.5	2.62	n	Yes	0.28±0.21	1.48±0.08	3.60±0.09	3.98±0.10	1.39±0.11	0.19±0.06	Seyfert
F13205+3853	0.428	J132248.41+383816.5	12.55			n	No							
F13209+6353	0.200	J132244.13+633724.9	12.21	6.8	6.72	I	Yes	0.60±0.06	4.14±0.28	5.07±0.11	7.58±0.11	3.98±0.08	1.11±0.06	Seyfert
F13210+3932	0.566	J132317.01+391626.5	12.93			n	Yes							
F13218+0552	0.203	J132419.89+053704.7	12.41	4.9	4.26	I	Yes							
F13231+6235	0.237	J132456.30+621958.1	12.31	3.9	2.85	I	Yes							
F13243+6308	0.242	J132608.51+625207.3	12.28			n	No	1.05±0.04	1.40±0.04	4.32±0.07	1.23±0.05	1.37±0.09		Starburst
F13342+3932	0.179	J133624.06+391731.0	12.37	6.4	6.94	I	Yes							
F13403−0038	0.326	J134251.61−005345.3	12.39			n	Yes							
F13408+4047	0.906	J134252.95+403201.6	13.47	151.6	136.55	n	Yes							
F13428+5608	0.037	J134442.16+555313.5	12.16	144.7	132.02	I	Yes	8.18±0.33	31.33±1.36	82.06±0.62	87.51±0.56	49.47±0.35	10.57±0.18	Seyfert
F13446+3727	0.215	J134651.82+371231.0	12.05	2.6	2.02	I	Yes	2.87±0.06	9.71±0.08	15.36±0.13	10.92±0.11	4.54±0.08	0.70±0.05	Seyfert
F13451+1232	0.121	J134733.36+121724.3	12.19		4859.88	II	Yes							
F13457+5702	0.209	J134732.49+564736.7	12.00		1.60	II	No							
F13469+5833	0.158	J134840.07+581851.9	12.29	3.1	3.02	I	Yes	0.43±0.06	0.31±0.05	3.45±0.09	2.79±0.07	1.47±0.08	0.19±0.03	Composite
F13479+3008	0.229	J135014.63+295318.1	12.18			n	No	3.29±0.05	3.07±0.05	13.62±0.12	3.75±0.05	3.33±0.07	0.35±0.03	Starburst
F13485+3739	0.248	J135043.17+372434.0	12.27	2.7	1.84	I	Yes	0.40±0.06	0.38±0.04	4.20±0.10	3.97±0.08	1.41±0.11	0.33±0.05	Composite
F13515+0317	0.278	J135404.79+030242.6	12.22		2.53	I	Yes	0.43±0.03	3.40±0.56	4.63±0.09	4.13±0.09	1.70±0.08	0.48±0.06	Seyfert
F13536−0108	0.199	J135612.65−012340.5	12.02		0.81	I	No	0.40±0.04	0.22±0.03	3.12±0.05	1.70±0.04	1.12±0.05	0.21±0.04	Composite
F13539+2920	0.109	J135609.99+290535.1	12.11	11.6	10.70	I	Yes	1.29±0.05	1.44±0.05	14.26±0.11	8.73±0.08	6.84±0.08	1.43±0.05	Composite
F13573+5429	0.253	J135908.54+541528.3	12.10		2.09	n	No							
F14014+3718	0.211	J140337.76+370355.5	12.10	2.4	1.96	III	Yes	2.69±0.06	2.70±0.04	14.58±0.13	5.70±0.08	3.55±0.07	0.40±0.05	Starburst
F14026+4341	0.323	J140438.80+432707.4	12.71		1.46	I	Yes							
F14041+0117	0.236	J140638.21+010254.6	12.48	14.6	9.19	n	Yes	1.02±0.03	2.73±0.12	49.51±0.07	1.68±0.10	2.21±0.07	0.99±0.07	Composite
F14060+2919	0.117	J140819.03+290447.0	12.13	9.3	7.86	I	Yes	6.38±0.09	5.03±0.09	45.34±0.32	20.29±0.17	13.78±0.13	1.82±0.06	Composite
F14060−0304	0.353	J140837.68−031900.8	12.52		2.14	n	Yes							
F14082+0205	0.201	J141049.55+015135.0	12.07		2.09	I	Yes							
F14088+0212	0.202	J141122.59+015815.1	12.05		1.02	I	Yes							

Table 1—Continued

IRAS name	z_{sdss}	SDSS name	$\log(\frac{L_{\text{FIR}}}{L_{\odot}})$	SNVSS 1.4GHz (mJy)	SFIRST 1.4GHz (mJy)	Note	NED	$f_{\text{H}\beta}$	$f_{\text{OIII}5007}$	$f_{\text{H}\alpha}$	$f_{\text{NII}6583}$	f_{SII}	$f_{\text{OI}6300}$	Note
(1)	(2)	(3)	(4)	(5)	(6)	(7)	(8)	(9)	(10)	(11)	(12)	(13)	(14)	(15)
F14146+2353	0.282	J141655.53+234018.2	12.14		1.28	n	No							
F14166+6514	0.364	J141753.69+650025.2	12.71			III	Yes							
F14167+4247	0.421	J141842.22+423343.3	12.70		1.25	n	Yes							
F14170+4545	0.150	J141858.85+453212.7	12.03	4.9	5.86	I	Yes							
F14202+2615	0.159	J142231.37+260205.1	12.36	9.8	8.31	II	Yes	5.28±0.07	4.72±0.07	29.29±0.24	13.13±0.13	8.74±0.10	0.98±0.05	Composite
F14204+4533	0.167	J142221.85+452011.9	12.01	7.4	7.87	n	Yes	4.68±0.63	4.77±0.26	28.24±0.22	12.61±0.12	8.21±0.12	1.20±0.06	Composite
F14248−0045	0.162	J142727.28−005841.1	12.18	5.4	3.51	III	Yes	0.77±0.04	0.60±0.05	9.73±0.11	5.56±0.08	3.31±0.08	0.58±0.06	Composite
F14298+5259	0.363	J143130.12+524532.8	12.43			n	Yes							
F14302+1243	0.332	J143245.00+122951.3	12.46			n	No							
F14312+2825	0.174	J143327.52+281159.8	12.22	6.0	5.63	I	Yes	0.60±0.08	5.07±0.09	8.20±0.09	7.47±0.08	2.68±0.07	0.53±0.04	Seyfert
F14315+2955	0.527	J143344.53+294248.0	12.82			n	No							
F14318−0252	0.187	J143425.31−030614.4	12.10			n	No	3.68±0.06	9.41±0.07	14.21±0.10	2.44±0.05	3.89±0.07	0.55±0.04	Starburst
F14330+0141	0.232	J143535.54+012834.8	12.16	14.6	15.08	I	Yes	0.16±0.03	1.54±0.05	1.82±0.05	1.83±0.05	0.93±0.09		Seyfert
F14336−0147	0.150	J143610.59−020055.6	12.02			I	No	1.04±0.15	1.61±0.33	4.17±0.06	1.24±0.05	0.44±0.04		Starburst
F14351+3553	0.362	J143715.26+354006.7	12.42			n	Yes							
F14374+0120	0.456	J144001.25+010743.2	12.80			n	Yes							
F14379+5420	0.268	J143930.59+540807.4	12.22	3.6	1.93	I	Yes	0.91±0.04	0.98±0.03	5.66±0.07	2.07±0.09	1.82±0.06	0.32±0.05	Starburst
F14390+6209	0.275	J144012.76+615633.2	12.31	3.4	2.88		Yes							
F14394+5332	0.105	J144104.38+532008.7	12.08	42.2	39.55	II	Yes							
F14402+0108	0.243	J144247.57+005532.0	12.08			n	No							
F14413+3730	0.259	J144319.55+371800.9	12.20		1.76	I	Yes							
F14483+0059	0.334	J145054.38+004646.8	12.37		1.29	I	No							
F14488+3521	0.206	J145054.16+350837.8	12.30	6.2	5.26	n	Yes	3.65±0.09	5.88±0.09	28.86±0.25	19.19±0.19	7.45±0.13	1.23±0.11	Composite
F14513−0235	0.209	J145355.90−024745.4	12.10		1.17	II	Yes	1.06±0.17	0.54±0.04	5.25±0.07	2.28±0.06	1.91±0.06	0.26±0.04	Starburst
F14541+3813	0.283	J145608.63+380038.6	12.01			n	No							
F14541+4906	0.247	J145549.42+485436.3	12.31	7.0	6.35	I	Yes	4.39±0.18	35.01±0.39	14.91±0.14	7.92±0.09	3.80±0.09	0.95±0.06	Seyfert
F14541+5734	0.301	J145531.90+572258.1	12.14			n	No	2.83±0.05	5.28±0.06	11.68±0.12	3.32±0.07	2.56±0.10	0.46±0.05	Starburst
F14560+0845	0.307	J145829.97+083400.3	12.36		2.28	I	No							
F15002+4945	0.337	J150150.52+493338.4	12.52	3.1	3.09	n	Yes	1.16±0.04	1.46±0.04	6.78±0.15	3.76±0.10	1.98±0.13	0.48±0.08	Composite
F15004+0351	0.218	J150259.01+034003.9	12.13		2.10	n	Yes	1.22±0.05	0.47±0.03	8.26±0.11	5.47±0.08	3.01±0.08	0.39±0.04	Composite
F15023+5404	0.280	J150351.02+535243.7	12.11			I	No	0.61±0.06	0.18±0.03	3.58±0.10	1.46±0.09	1.05±0.09	0.00±0.00	Starburst

Table 1—Continued

IRAS name	z_{sdss}	SDSS name	$\log(\frac{L_{\text{FIR}}}{L_{\odot}})$	SNVSS 1.4GHz (mJy)	SFIRST 1.4GHz (mJy)	Note	NED	$f_{\text{H}\beta}$	$f_{\text{OIII}5007}$	$f_{\text{H}\alpha}$	$f_{\text{NII}6583}$	f_{SII}	$f_{\text{OI}6300}$	Note
(1)	(2)	(3)	(4)	(5)	(6)	(7)	(8)	(9)	(10)	(11)	(12)	(13)	(14)	(15)
F15034+4444	0.465	J150517.72+443244.0	12.56		2.30	n	No							
F15043+5754	0.151	J150539.56+574307.3	12.16	2.4	2.64	I	Yes	1.29±0.13	1.11±0.18	8.87±0.09	3.62±0.06	3.00±0.07	0.32±0.05	Starburst
F15070+4100	0.307	J150858.61+404917.1	12.24			I	Yes							
F15097−0133	0.207	J151218.48−014430.2	12.10	3.3	3.00	n	No	1.51±0.10	1.45±0.04	7.94±0.10	3.64±0.06	2.89±0.06	0.39±0.08	Composite
F15111+2458	0.220	J151318.04+244655.3	12.19		3.19	I	No	1.39±0.70	5.64±0.36	8.26±0.11	7.51±0.10	4.30±0.08	0.89±0.05	Seyfert
F15177+5909	0.296	J151859.47+585828.7	12.28			n	No							
F15206+3342	0.125	J152238.10+333135.8	12.18	10.7	9.96	n	Yes	27.69±0.94	80.74±1.13	149.06±0.95	34.49±0.71	23.51±0.18	4.88±0.29	Composite
F15206+3631	0.152	J152234.86+362058.6	12.04	4.8	4.82	II	Yes	0.48±0.11	1.62±0.08	6.39±0.10	10.20±0.11	3.99±0.08	1.14±0.06	Ambiguity
F15222+2405	0.318	J152424.49+235524.0	12.31			n	No							
F15225+2350	0.138	J152443.88+234010.2	12.15	6.6	5.53	I	Yes	0.84±0.03	1.73±0.15	8.53±0.08	4.56±0.05	2.95±0.06	0.40±0.03	Composite
F15250+3608	0.055	J152659.44+355837.1	12.01	14.5	13.06	I	Yes	4.63±0.18	5.11±0.12	26.45±0.22	12.31±0.15	10.05±0.14	1.99±0.09	Composite
F15261+5502	0.229	J152726.65+545151.2	12.22		1.50	I	Yes	0.90±0.04	0.93±0.03	4.35±0.06	1.60±0.04	1.72±0.06	0.29±0.03	Starburst
F15296+3612	0.344	J153135.34+360242.7	12.36			n	Yes							
F15320+0325	0.206	J153431.02+031527.7	12.05	4.0	2.95	I	No							
F15330+4439	0.250	J153447.05+442923.4	12.04			II	No	0.82±0.06	0.46±0.03	3.97±0.06	1.38±0.05	1.07±0.09	0.29±0.06	Starburst
F15390+3913	0.239	J154049.23+390350.8	12.02		1.61	n	Yes	7.61±0.07	21.15±0.15	30.79±0.21	5.98±0.07	5.87±0.09	1.04±0.04	Starburst
F15432+3502	0.516	J154510.96+345247.0	12.81	18.5	15.93	n	Yes							
F15437+4647	0.228	J154518.05+463838.1	12.04	3.5	3.67	II	No							
F15439+4855	0.399	J154530.24+484609.1	12.58	3.6	2.11	II	Yes							
F15458+0041	0.252	J154823.32+003212.1	12.05		1.99	n	No	0.35±0.03	5.53±0.30	2.32±0.04	2.89±0.04	1.18±0.07	0.22±0.03	Seyfert
F15478+5014	0.197	J154916.28+500536.4	12.11	3.2	2.44	n	Yes	1.45±0.06	0.75±0.04	8.75±0.10	4.56±0.07	2.50±0.07	0.26±0.03	Composite
F15529+4545	0.517	J155433.22+453646.4	12.81		1.32	I	Yes							
F15531+2513	0.185	J155519.53+250433.4	12.02			II	No	0.88±0.06	0.50±0.04	5.52±0.06	3.12±0.06	2.12±0.07	0.26±0.04	Composite
F15577+3816	0.218	J155930.40+380838.7	12.14	3.1	2.41	I	Yes	2.11±0.06	25.12±0.62	9.12±0.10	4.93±0.08	2.96±0.08	0.70±0.04	Seyfert
F15583+4002	0.218	J160006.09+395403.0	12.06		2.02	I	Yes							
F16019+0828	0.228	J160418.83+082037.2	12.21			I	No	3.00±0.03	4.29±0.04	13.69±0.08	3.82±0.04	3.52±0.05	0.43±0.02	Starburst
F16031+4222	0.223	J160446.69+421415.3	12.11		1.75	n	No							
F16075+2838	0.170	J160933.41+283058.4	12.16	4.3	4.80	II	Yes							
F16078+2645	0.190	J160958.54+263739.6	12.16			n	No							
F16098+2624	0.184	J161153.76+261646.2	12.08		1.67	I	No							
F16109+2318	0.373	J161307.19+231101.7	12.68			n	No							

Table 1—Continued

IRAS name	z_{sdss}	SDSS name	$\log(\frac{L_{\text{FIR}}}{L_{\odot}})$	SNVSS 1.4GHz (mJy)	SFIRST 1.4GHz (mJy)	Note	NED	$f_{\text{H}\beta}$	$f_{\text{OIII}5007}$	$f_{\text{H}\alpha}$	$f_{\text{NII}6583}$	f_{SII}	$f_{\text{OI}6300}$	Note
(1)	(2)	(3)	(4)	(5)	(6)	(7)	(8)	(9)	(10)	(11)	(12)	(13)	(14)	(15)
F16116+0638	0.241	J161407.70+063114.1	12.14		1.32	I	No							
F16117+4904	0.241	J161315.95+485721.9	12.04	4.8	4.32	n	No							
F16122+1531	0.308	J161431.72+152421.9	12.42	24.2	20.27	n	No							
F16126+1953	0.252	J161448.24+194609.8	12.27		2.93	I	No							
F16133+2107	0.091	J161534.13+210019.7	12.00	9.4	11.24	I	Yes	0.61±0.08	0.99±0.06	6.63±0.08	6.20±0.08	4.85±0.09	1.14±0.06	LINERs
F16148+2104	0.415	J161657.59+205746.6	12.85			II	No							
F16172+4432	0.335	J161849.25+442517.3	12.41	3.0	3.09	I	No							
F16264+3157	0.361	J162824.02+315028.3	12.37		1.51	n	Yes	0.06±0.02	1.57±0.03	1.15±0.14	1.30±0.13	1.02±0.12	0.14±0.04	Seyfert
F16300+1558	0.242	J163221.37+155145.5	12.77	7.5	5.93	I	Yes	0.25±0.03	0.73±0.04	3.85±0.07	2.25±0.06	1.97±0.10	0.44±0.05	Seyfert
F16301+4617	0.329	J163134.12+461050.6	12.29		1.04	I	Yes	1.10±0.06	0.84±0.03	5.53±0.09	2.44±0.08	1.51±0.10	0.15±0.04	Composite
F16403+2537	0.160	J164223.46+253147.6	12.03		4.40	n	No	3.36±0.08	2.05±0.08	25.16±0.25	14.10±0.16	8.72±0.14	1.09±0.08	Composite
F16413+3954	0.594	J164258.81+394837.0	13.39	7098.6	6598.61	n	Yes							
F16474+3430	0.113	J164914.09+342513.2	12.22	11.1		II	Yes	1.54±0.05	1.00±0.05	7.71±0.09	3.14±0.05	2.52±0.06	0.26±0.03	Starburst
F16533+6216	0.106	J165352.11+621149.7	12.02	16.5	14.43	n	Yes	5.90±0.09	3.13±0.07	36.78±0.24	20.22±0.16	12.02±0.11	1.67±0.06	Composite
F17051+3824	0.168	J170653.27+382007.0	12.23	4.4	4.30	I	Yes	0.24±0.07	0.71±0.07	2.23±0.06	3.22±0.06	2.25±0.09	0.50±0.06	LINERs
F17081+3300	0.279	J171000.75+325658.0	12.20			n	Yes	0.87±0.03	3.29±0.05	6.42±0.08	4.89±0.07	1.74±0.07	0.39±0.04	Seyfert
F17175+6603	0.292	J171737.96+655939.3	12.25			n	Yes							
F17214+2845	0.241	J172322.64+284249.6	12.32			n	No	0.91±0.03	0.43±0.02	4.99±0.06	1.80±0.04	1.54±0.06	0.21±0.04	Starburst
F17234+6228	0.240	J172351.74+622519.6	12.14	5.7	1.93	n	Yes							
F20522−0120	0.173	J205450.55−010831.3	12.22			I	No	4.41±0.06	6.20±0.07	17.96±0.12	5.71±0.06	4.68±0.07	0.60±0.03	Starburst
F21045+1058	0.166	J210654.94+111007.8	12.09			I	No	0.14±0.03	0.35±0.04	2.52±0.05	1.97±0.04	1.34±0.07	0.55±0.06	Ambiguity
F21234−0023	0.458	J212559.03−001044.4	13.08			n	Yes							
F21461+1117	0.151	J214833.44+113147.8	12.02	10.6		I	Yes							
F22015+0045	0.289	J220405.30+005917.5	12.31			n	Yes	3.92±0.05	7.14±0.07	17.32±0.17	5.07±0.09	4.63±0.13	1.07±0.05	Ambiguity
F22098−0748	0.143	J221232.09−073334.0	12.00	4.8	4.63	I	Yes	1.67±0.06	0.89±0.06	12.68±0.11	7.21±0.08	3.99±0.08	0.48±0.05	Composite
F22239−0916	0.298	J222634.05−090106.1	12.39		1.72	n	Yes	0.20±0.03	0.60±0.05	2.78±0.07	2.24±0.07	0.36±0.07	0.10±0.04	Ambiguity
F22532+1233	0.356	J225545.29+124943.4	12.70			I	Yes							
F23051−0100	0.362	J230743.26−004404.0	12.55			n	No							
F23254+1429	0.156	J232800.79+144646.7	12.02			n	No							

Note. — Column (1) is IRAS name; Column (2) is the redshift from SDSS; Column (3) lists SDSS name of the object; Column (4) is infrared luminosity; Column (5) and (6) give radio fluxes from NVSS and FIRST, respectively; Column (7) is the class (I, II, III) for interaction features, “n” stands for not clear. Column (8) is NED identifications. “Yes”: the redshift or/and the counterpart provided in the NED is consistent with ours. “No”: the redshift is not listed in the NED. Column (9) to (14) list the fluxes of H_β , [OIII]5007, H_α , [NII]6583, [SII]6716+6731, [OI]6300, all in unit of $10^{-15}\text{ergs}^{-1}\text{cm}^{-2}$; Column (15) is the note for the type of the galaxy according to the BPT diagram.

Table 2. The parameters of Type I ULIRG sample.

IRAS name	z	$f_{(5100\text{\AA})}$	FWHM H_{β} km s ⁻¹	FWHM [OIII] km s ⁻¹	FWHM [OIII] NL core km s ⁻¹	FWHM [SII] km s ⁻¹	M _{BH} 10 ⁷ M _⊙	$\frac{L_{\text{bol}}}{L_{\text{Edd}}}$	log($\frac{L_{\text{IR}}}{L_{\odot}}$)	quality
(1)	(2)	(3)	(4)	(5)	(6)	(7)	(8)	(9)	(10)	(11)
F01572+0009	0.163	134.88 ^{+25.23} _{-22.09}	3141	689	504 ⁺⁷ ₋₈	592 ⁺²⁶ ₋₂₆	10.21±2.65	0.35	12.52	1
F02486-0714	0.327	17.42 ^{+9.87} _{-6.92}	1799	748	564 ⁺¹³ ₋₁₄	430 ⁺²⁸ ₋₂₈	2.51±1.01	0.89	12.32	1
F07548+4227	0.211	59.55 ^{+12.54} _{-10.81}	3691	449	357 ⁺⁶ ₋₅	412 ⁺¹² ₋₁₂	12.15±3.06	0.23	12.13	1
F07578+5148	0.196	22.71 ^{+10.53} _{-7.81}	3201	461	385 ⁺¹¹ ₋₁₂	405 ⁺³² ₋₃₂	4.59±1.53	0.20	12.07	1
F08209+2458	0.234	10.35 ^{+10.63} _{-6.00}	949	886	886		0.32±0.24	1.93	12.19	2
F08238+0752	0.311	66.30 ^{+15.92} _{-13.47}	3547	724	669 ⁺³¹ ₋₃₀		20.53±6.66	0.37	12.41	1
F08407+2630	0.257	31.67 ^{+10.16} _{-8.18}	3156	509	462 ⁺⁹ ₋₈	369 ⁺⁵⁰ ₋₅₀	7.93±2.25	0.29	12.10	1
F08435+3141	0.386	7.72 ^{+9.90} _{-5.00}	2110	2185	2185		2.66±2.14	0.55	12.46	2
F08542+1920	0.331	41.29 ^{+11.99} _{-9.85}	4362	2084	2084		25.40±8.08	0.21	12.46	2
F09005+2253	0.290	15.97 ^{+8.34} _{-5.99}	7577	413	413 ⁺⁹ ₋₉	390 ⁺²⁵ ₋₂₅	35.62±13.16	0.04	12.24	1
F09008+3643	0.288	6.04 ^{+13.30} _{-4.98}	2552	1485	1485		2.21±3.01	0.26	12.55	2
F09105+4108	0.442	12.52 ^{+7.92} _{-5.37}	1362	659	492 ⁺³ ₋₃		1.81±0.81	1.80	12.87	1
F09220+2759	0.531	5.86 ^{+8.91} _{-4.14}	2335	970	641		4.38±4.17	0.54	12.92	2
F09438+4735	0.539	21.67 ^{+15.28} _{-9.99}	4804	784	784		42.08±22.50	0.22	13.01	2
F09591+2045	0.357	13.42 ^{+9.39} _{-6.16}	5479	701	265		22.48±11.07	0.09	12.50	2
F10015-0018	0.289	13.09 ^{+8.81} _{-5.86}	1562	736	265	239 ⁺²⁴ ₋₂₄	1.34±0.61	0.94	12.52	2
F10026+4347	0.179	80.56 ^{+22.74} _{-18.73}	2627	1772	1772		5.92±1.62	0.45	12.08	2
F10106+2227	0.274	27.74 ^{+9.80} _{-7.73}	3752	1048	1048 ⁺⁶⁹ ₋₇₀	277 ⁺³² ₋₃₃	11.30±3.39	0.21	12.15	1
F10234+3052	0.340	29.43 ^{+12.75} _{-9.63}	2980	665	517 ⁺¹⁹ ₋₁₉	448 ⁺⁸⁷ ₋₈₇	10.02±3.60	0.41	12.47	1
F10372+4801	0.486	9.39 ^{+9.44} _{-5.37}	1109	641	559 ⁺⁶ ₋₅		1.16±0.84	2.65	12.81	1
F10531+5531	0.256	17.81 ^{+11.56} _{-7.77}	3671	557	557 ⁺³⁵ ₋₃₅	304 ⁺⁵⁵ ₋₅₆	7.51±3.27	0.17	12.01	1
F10538+3309	0.457	5.43 ^{+9.49} _{-4.08}	2841	461	461		4.97±5.44	0.31	12.62	2
F11028+3442	0.509	99.27 ^{+23.88} _{-20.19}	4347	2311	2311		80.14±36.16	0.45	12.86	2
F11066+4242	0.232	16.16 ^{+11.20} _{-7.37}	6845	527	527 ⁺¹⁹ ₋₁₉		21.47±9.91	0.04	12.11	1
F11070+4249	0.261	14.34 ^{+10.39} _{-6.73}	1230	904	725 ⁺¹³ ₋₁₄	534 ⁺¹⁷ ₋₁₈	0.76±0.36	1.44	12.34	1
F11134+0225	0.211	61.01 ^{+15.93} _{-13.28}	3398	790	467 ⁺³³ ₋₃₂		10.45±2.82	0.28	12.01	1
F11162+6020	0.264	18.40 ^{+12.65} _{-8.35}	1535	1156	779		1.40±0.64	1.03	12.55	2
F11163+3207	0.261	15.03 ^{+11.59} _{-7.34}	1369	814	570 ⁺¹⁶ ₋₁₆		0.97±0.65	1.18	12.22	1
F11206+3639	0.242	11.77 ^{+9.45} _{-5.90}	990	641	506 ⁺⁹ ₋₉		0.39±0.21	1.94	12.42	1
F11307+0449	0.248	19.10 ^{+10.23} _{-7.31}	2593	335	335 ⁺¹⁵ ₋₁₅	261 ⁺⁸³ ₋₈₃	3.74±1.40	0.35	12.12	1
F11394+0108	0.245	14.81 ^{+8.76} _{-6.07}	1142	359	328 ⁺⁹ ₋₈	427 ⁺⁹ ₋₁₀	0.61±0.27	1.61	12.22	1
F11417+1151	0.271	100.11 ^{+24.62} _{-20.80}	6058	581	440 ⁺¹⁶ ₋₁₅		63.47±21.14	0.13	12.33	1
F11553-0259	0.215	25.82 ^{+12.13} _{-8.98}	2534	1180	961 ⁺¹⁷ ₋₁₇		3.53±1.19	0.36	12.06	1
F11557+1342	0.439	30.18 ^{+11.52} _{-8.95}	3629	311	268 ⁺⁸ ₋₈		21.78±8.13	0.36	12.66	1
F12043+5215	0.398	8.26 ^{+8.80} _{-4.84}	2012	1401	1401		2.63±1.80	0.64	12.51	2
F12136+3919	0.334	8.90 ^{+9.17} _{-5.17}	4036	455	455 ⁺³⁰ ₋₃₁		8.64±5.68	0.14	12.70	1
F12433+6540	0.320	33.34 ^{+11.95} _{-9.39}	3097	365	280 ⁺¹⁸ ₋₁₉	197 ⁺²⁸ ₋₂₈	10.71±3.50	0.38	12.36	1
F12489+6619	0.282	62.99 ^{+16.40} _{-13.68}	3074	299	299 ⁺¹² ₋₁₂	371 ⁺³⁹ ₋₃₉	13.02±4.06	0.44	12.17	1
F13210+3932	0.566	12.08 ^{+9.09} _{-5.77}	3042	695	695		12.69±6.94	0.45	12.93	2
F13342+3932	0.179	58.35 ^{+17.40} _{-14.24}	5789	503	467 ⁺⁶ ₋₇	435 ⁺¹³ ₋₁₃	23.59±6.38	0.08	12.37	1
F13403-0038	0.326	48.91 ^{+11.42} _{-9.69}	4456	1209	865 ⁺⁶⁰ ₋₅₉		28.76±8.88	0.22	12.39	1
F13451+1232w	0.121	22.59 ^{+10.78} _{-7.95}	2249	1383	1087		1.18±0.42	0.27	12.19	2

Table 2—Continued

IRAS name	z	$f_{(5100\text{\AA})}$	FWHM H_β km s ⁻¹	FWHM [OIII] km s ⁻¹	FWHM [OIII] NL core km s ⁻¹	FWHM [SII] km s ⁻¹	M_{BH} $10^7 M_\odot$	$\frac{L_{\text{bol}}}{L_{\text{Edd}}}$	$\log(\frac{L_{\text{IR}}}{L_\odot})$	quality
(1)	(2)	(3)	(4)	(5)	(6)	(7)	(8)	(9)	(10)	(11)
F14026+4341	0.323	$225.42^{+42.23}_{-37.00}$	5490	2084	2084		109.45 ± 45.99	0.26	12.71	2
F14082+0205	0.201	$14.00^{+9.76}_{-6.41}$	2161	742	742^{+24}_{-24}	192^{+11}_{-11}	1.61 ± 0.78	0.37	12.07	1
F14166+6514	0.364	$11.46^{+9.80}_{-5.97}$	3775	533	533^{+28}_{-29}		9.97 ± 5.55	0.19	12.71	1
F14167+4247	0.421	$61.33^{+18.06}_{-14.74}$	5346	515	412^{+20}_{-20}		68.55 ± 26.57	0.21	12.70	1
F14302+1243	0.332	$9.75^{+9.52}_{-5.49}$	4677	365	346^{+9}_{-10}		12.16 ± 7.66	0.11	12.46	1
F14315+2955	0.527	$28.53^{+12.28}_{-9.25}$	5973	581	412^{+24}_{-24}		74.42 ± 31.04	0.15	12.82	1
F14390+6209	0.275	$54.52^{+12.92}_{-10.95}$	3375	479	346^{+8}_{-8}	429^{+17}_{-16}	13.88 ± 4.03	0.34	12.31	1
F14394+5332	0.105	$43.82^{+15.58}_{-12.31}$	1827	1826	1828		0.97 ± 0.27	0.46	12.08	2
F14402+0108	0.243	$9.56^{+7.95}_{-4.90}$	4097	323	323^{+10}_{-11}		5.96 ± 3.21	0.10	12.08	1
F14541+3813	0.283	$28.30^{+12.38}_{-9.30}$	7045	569	492^{+13}_{-13}	551^{+109}_{-109}	42.20 ± 14.44	0.06	12.01	1
F15320+0325	0.206	$22.95^{+10.32}_{-7.72}$	904	581	254^{+12}_{-12}		0.39 ± 0.14	2.63	12.05	1
F15432+3502	0.516	$51.61^{+16.14}_{-13.05}$	3817	1449	478^{+67}_{-67}		42.30 ± 17.69	0.46	12.81	1
F15437+4647	0.228	$35.04^{+14.00}_{-10.78}$	4972	814	465^{+35}_{-35}	491^{+16}_{-16}	17.74 ± 6.01	0.11	12.04	1
F15439+4855	0.399	$82.80^{+20.52}_{-17.28}$	5628	2090	2090		84.43 ± 32.91	0.20	12.58	2
F15529+4545	0.517	$8.92^{+11.94}_{-5.93}$	2931	772	587^{+32}_{-31}		8.57 ± 7.32	0.39	12.81	1
F16122+1531	0.308	$13.71^{+8.40}_{-5.75}$	2041	2138	487	538^{+21}_{-20}	2.56 ± 1.12	0.60	12.42	2
F16172+4432	0.335	$57.28^{+15.41}_{-12.83}$	5150	497	391^{+11}_{-10}		43.97 ± 14.72	0.18	12.41	1
F16413+3954	0.594	$271.96^{+38.50}_{-34.84}$	4439	1126	1126		194.01 ± 110.28	0.74	13.39	2
F17175+6603	0.292	$31.56^{+10.58}_{-8.42}$	5701	641	403^{+24}_{-24}	511^{+69}_{-70}	30.86 ± 9.34	0.10	12.25	1
F17234+6228	0.240	$7.51^{+12.34}_{-5.51}$	1113	425	385^{+9}_{-9}	728^{+36}_{-36}	0.37 ± 0.65	1.28	12.14	1

Note. — Column (1) is IRAS name, Column (2) lists redshift, Column (3) is continuum flux at 5100 Å corrected by use of $F_\lambda(5100\text{\AA})_{\text{rest}} = (1+z)F_\lambda((1+z)5100\text{\AA})_{\text{obs}}$, where z is the redshift, and the unit is $10^{-17} \text{ergs}^{-1} \text{cm}^{-2} \text{\AA}^{-1}$. Column (4) to (7) list the FWHM of broad component of H_β , FWHM of [OIII]5007 profile, the [OIII]5007 narrow line core, as well as the [SII]6716, if available. Column (8) is the derived BH mass, Column (9) is the Eddington ratio, Column (10) is the infrared luminosity, Column (11) indicates the quality of [OIII]5007 FWHM, “1”: the fitting result is reliable. “2”: the FWHM can not be well fitted due to the low quality of the spectra or suffer serious absorptions around the emission lines.